OUKA
The University of Osaka
Institutional Knowledge Archive

| | |
|---|---|
| Title | Force and torque effect of MRI scanner on dental metals |
| Author(s) | Kitisriworapan, Wiranut |
| Citation | 大阪大学, 2023, 博士論文 |
| Version Type | VoR |
| URL | https://doi.org/10.18910/92998 |
| rights | |
| Note | |

*The University of Osaka Institutional Knowledge Archive : OUKA*

https://ir.library.osaka-u.ac.jp/

The University of Osaka

*Manuscript for Ph.D. final examination*

# Force and torque effect of MRI scanner on dental metals

Wiranut Kitisriworapan

*Department of Oral and Maxillofacial Radiology*

*Osaka University Graduate School of Dentistry*

（Supervised by Professor Shumei Murakami）

September 2023

## INTRODUCTION

Imaging diagnosis using MRI is becoming increasingly important in the medical and dental fields. Because MRI is a nonionizing radiation imaging modality (1), there is no radiation exposure to the patient. Other advantages of MRI are a superior soft tissue contrast compared to the other radiological imaging modalities (2) and the allowance for selecting of optional tomographic planes (3). Therefore, MRI is an indispensable modality for diagnosing oral and maxillofacial lesions.

In order to perform MR imaging, three independent magnetic fields are used, namely the static magnetic field, the radiofrequency electromagnetic field, and spatial-encoding magnetic fields (1,4). These magnetic fields have unique safety concerns and risks that can affect the patients, the image diagnosis, and the medical electronic devices (1). The major risks related to a static magnetic field are magnetically induced displacement force and torque on metal objects (5,6). The main risk associated with the radiofrequency electromagnetic field is heat generation on the tissues or metal objects (5,7). Moreover, there are many risks associated with the spatial-encoding magnetic fields. For example, the auditory sounds or noises associated with the MR imaging process and the inducing neuroexcitation of nerves (5).

Among many MRI-associated risks, the most immediate risk that could be occur when the patient enter the MRI room is the displacement force caused by the static magnetic field (8). This force attracts the metal object to the MRI magnet, causing the translation of the object from the previous position. Because the static magnetic field is generated by the superconducting coils that are generally always on, the safety risks caused by this field can occur at any time, even if during the non-scanning

period (1). The displacement force is determined by the strength of the static magnetic field at the location where the object is found, as well as the spatial gradient across the object at that position in space (5). The maximum displacement force will occur at the locations at the entrance of the gantry (1,4,9), where the patient will pass before entering the gantry, because the spatial gradient tends to be the greatest there. However, inside the gantry, near the isocenter, the magnetic field becomes very uniform and the spatial gradient is zero, therefore, it was said that the displacement force will become zero there (4).

As explained previously, another risk related to the static magnetic field is the magnetically induced torque. The metal objects in the magnetic field with asymmetric aspect ratios would be received the rotating force or torque that tends to align their long axes parallel to the direction of the static magnetic field. The stronger the static magnetic field in that particular position, the stronger the torque-related forces (5). It was said that torque would be maximal in the region around the MRI magnet isocenter (1).

Because MRI involves magnetic field strengths that are much larger than typical everyday experience, so regular objects may behave unreasonably and unexpectedly near the scanner. Objects behavior in such conditions depends on the component determining their magnetic properties (4,10,11). Metallic materials can be classified according to their degree of magnetic susceptibility as ferromagnetic (materials that have a large, positive susceptibility to an external magnetic field such as iron, cobalt, and nickel), paramagnetic (materials that have a small, positive susceptibility to magnetic fields such as chromium, manganese, and aluminum), or diamagnetic (materials that have a weak, negative susceptibility to magnetic fields such as copper, gold, zinc, lead, and carbon) (8,12,13).

In order to define the MRI compatibility to medical implants and devices, there are three labeling terminologies recognized by the U.S. Food and Drug Administration (FDA) namely, MR safe, MR conditional, and MR unsafe. MR safe means an item that poses no known hazards in all MR imaging environments, including items that are nonconducting, nonmetallic, and nonmagnetic, such as a plastic Petri dish. MR conditional means an item that has been demonstrated to pose no known hazards in a specified MR environment with specified conditions of use. Lastly, MR unsafe means an item that is known to pose hazards in all MR environments, including magnetic items such as a pair of ferromagnetic scissors (9,14,15).

In dentistry, several dental materials such as dental restoration, prostheses, and orthodontic appliances consist of various kinds of metals and metal alloys that may have interactions with MRI (17,16), such as image artifacts, heating, magnetically induced displacement force and torque. There are many previous studies that have examined the image artifacts and heating generated by dental metal materials (16,18,19,20). Regarding the magnetically induced displacement force and torque, some previous studies said that patients with metallic foreign objects are often prohibited from MRI scanning because these objects may be dislodged due to these forces (16, 17). Moreover, removable dentures should be removed before an MRI scan to prevent the risk of movement that can cause harm to the patient as well as the device (8). It was reported that MRI also has been used in orthodontic treatments to image the temporomandibular joint (11,21). The removable orthodontic appliances must to be removed before performing the MRI examination. However, fixed orthodontic appliances such as brackets and wires often cause a dilemma (22). There is inadequate evidence that they are needed to be removed before the MRI scan and insufficient evidence to suggest that they are dislodged during

the scan (11). Therefore, it is still unclear for radiologists and the orthodontists whether removing fixed orthodontic appliances is mandatory before the scanning.

Klocke et al. performed two studies on the magnetic field interaction of orthodontic wires using the 1.5 Tesla (23) and 3 Tesla MRI (24); the result of the displacement forces on all the tested steel orthodontic arch wires from the study at 3 T MRI were higher than the displacement forces of the same tested materials from the study at 1.5 T MRI. However, they measured torque by the qualitative scale and the torque results on steel arch wires of the study at 1.5 T were the same as those at 3T, except for only one type of arch wire.

Regarding metal dental devices or materials, these days, there are cases where the patient forgets to remove them, there is no instruction from the doctor, or it is unknown whether or not they can be removed as explained previously. Moreover, some previous studies have shown the displacement force and torque applied to dental metals. However, there were many problems or limitations, such as the limited number of metals tested and limited measurement locations.

## OBJECTIVES

1) To measure the magnetically induced displacement force and torque on materials including dental materials and some of household items at each spatial point in the examination room for an MRI scanner with a static magnetic field strength of 3 Tesla.
2) To examine a relationship between the magnetically induced displacement force and torque and a magnetic flux density

## MATERIALS AND METHODS

The 3 Tesla superconducting MRI scanner SIGNA$^{TM}$ Premier (GE HealthCare, USA) was used in this study.

### 1) Magnetic flux density measurement

#### 1.1 Magnetic flux density outside the scanner in the MRI room

The magnetic flux density outside the scanner was measured by an AC/DC Magnetic Meter LUTRON MG-3002 (LUTRON, Taiwan). At each measuring point, the tip of the meter was pointing upward and the probe was attached to the rotatable wood pole. Then, the pole was rotated and the maximum value was recorded. The measurement at each point was performed six times.

The measuring points were two-dimensionally 25 cm grid intersection, at three of the heights, namely -100 cm (ground level), 0 cm (patient table level), and 50 cm (patient height level) (Fig.1).

The magnetic flux density was measured along the three axes (x, y, z) (Fig.1). The z-axis was parallel to the central axis or the centerline of the MRI gantry, positive z direction was pointing out of the gantry entrance. The x-axis was parallel to the surface of the scanner horizontally, positive x direction was on the right side of the scanner when looking from the opposite wall and facing through the scanner. The y-axis was the vertical levels perpendicular to the x-axis, represented by three of the heights as explained previously.

### 1.2 Magnetic flux density along the gantry centerline, inside and outside of the gantry

The magnetic flux density along the gantry centerline, inside and outside of the gantry was measured by a METROLAB Precision NMR Teslameter PT2025 (METROLAB, Switzerland). The meter was placed on the patient table and the table was moved inside and outside the gantry.

The spatial gradient of magnetic field and the product of the magnetic flux density and the spatial gradient were calculated from the measured magnetic flux density. The spatial gradient is the change in the strength of the magnetic field with respect to distance and is measured in Tesla per meter (T/m) (4).

## 2) Displacement force measurement

The displacement force was measured according to the ASTM F2052-15 (25).

From the ASTM guideline, the deflection angles of the materials were measured, then the displacement force was calculated from the deflection angle and the weight of the tested material.

At first, the tested material was suspended by a light string. The weight of the string is less than 1 % of the weight of the tested material. The other end of the string was set at the center of a protractor apparatus made by ourselves (Fig.2). As a reference when measuring the deflection angle, a reference object made of lead, that was not pulled by the MRI magnet, was set at the center of the protractor by another light string. After that, the deflection angle between the two threads was measured.

In this study, in order to calculate the displacement force not only the force along the centerline of the gantry but also the displacement force at other positions in the MRI room, the origin of the attraction force by the MRI magnet was investigated by the preliminary tested and the equation for calculation of the displacement force of the ASTM F2052-15 was modified as the equation below. (W is weight of tested material; θ is deflection angle; x, y, z are distances along coordinate system.)

$$\text{Displacement force} = \frac{\sqrt{x^2 + (y-100)^2 + z^2} \times W \times \tan\theta}{\sqrt{x^2 + z^2} - (y-100) \times \tan\theta}$$

**2.1 Displacement force, outside the scanner in the MRI room**

The measured points and the height levels were same as for the magnetic flux density measurement, two-dimensionally 25 cm grid intersection, at three of the heights, namely -100 cm (ground level), 0 cm (patient table level), and 50 cm (patient height level).

The representative tested material is a paperclip, it was made of magnetic stainless steels and was ferromagnetic (26). This material was selected to be the representative material in order to observe the tendency of displacement forces on ferromagnetic material in the MRI magnetic field.

**2.2 Displacement force along the gantry centerline, inside and outside of the gantry**

The displacement force was measured along the patient bed at every 5 cm along z-axis. The representative tested material is a plastic bracket. This material was selected to be the representative

material because, in our preliminary test, it showed the maximum deflection angle less than 70 degrees inside the gantry and was not touched the wall of the gantry during moving inside the gantry.

**2.3 Displacement force of various materials (dental materials & household items) at two points along the gantry centerline level, 25 and 50 cm outside the gantry entrance**

The deflection angle was measured along the patient bed and the displacement force was calculated. The number of tested materials were 44, including dental materials and household items. The list of all tested materials was showed in the Table 1.

**3) Torque measurement**

Torque was measured according to the ASTM F2213-17 by adaptation of the Pulley method (27). The measurement apparatus consisting of the non-friction rotatable plate was made by ourselves (Fig.3).

The measurement was performed at 6 positions inside the gantry, including at the isocenter of the gantry (0), 10, 20, 30, 40, and 50 cm along the gantry centerline level.

Firstly, the tested material was fixed on the rotatable plate of the apparatus and the long axis of the material was set 45 degrees to the direction of the static magnetic field. Then, the force induced by torque was measured at balance, where the long axis of the material was parallel to the static magnetic field. The torque on an asymmetric object in the static magnetic field depends on the deflection angle

between the long axis of the object and the direction of the static magnetic field. And the maximum torque is found at the angle of 45 degrees (28). Therefore, the pulling force was measured when the object formed the angle of 45 degrees to the static magnetic field. (Fig.3) In order to change the direction of the material long axis, the rotatable plate was rotated by adding the non-magnetic object to the end of the string that attached to the plate. The total weight of the non-magnetic objects was measured by the digital scale and then torque was calculated by multiplying the weight of the non-magnetic objects with the radius of the rotatable plate (4 cm).

The number of tested materials were 14, including dental materials and household items. The list of all tested materials was showed in the Table 2. All orthodontic arch wires were cut into 3 cm length in order to place on the rotatable plate without interference.

**Statistical analysis**

All measurements were performed six times. The means and standard deviation were calculated. The displacement force applied to the paper clip was statistically compared at each point with an average of ten mN or more. The displacement force applied to the plastic bracket was statistically compared at each point with an average of one mN or more. The comparison between data was performed by Tukey's test, $p<0.01$ and SPSS® ver. 28

## RESULTS

### 1) Magnetic flux density measurement

#### 1.1 Magnetic flux density outside the scanner in the MRI room

The bar charts and the tables representing the distribution of the measured magnetic flux density outside the scanner at the three heights, including -100 cm (ground level), 0 cm (patient table level) and 50 cm (patient height level), were showed in Fig.4 to Fig.6 and Table3 to Table5.

At the height of -100 cm (ground level), there is a table base, which is the component of the MRI scanner for connecting to the patient bed, fixed on the floor. Therefore, some points in this area could not be measured. The magnetic flux density values at the height of -100 cm (Fig.4, Table 3) were decreased while the distances along the z-axis away from the scanner increased. However, the values along the center line of the z-axis were lower than those along the following lines on the right and left sides until the distance was 75 cm away from the scanner. The right and left symmetry was confirmed using linear regression, and the coefficient of determination ($R^2$) was 0.998. The maximum magnetic flux density value at the height of -100 cm was 60.1 milli-tesla (mT) or 0.06 Tesla (T) at the position 25 cm away from the gantry entrance and 50 cm on the right side of the gantry.

The magnetic flux density values at the height of 0 cm (patient table level) (Fig.5, Table 4) rapidly decreased while the distances along the z-axis away from the scanner increased. The magnetic flux densities were rapidly attenuated at the edge of the gantry. The values decreased with increasing distance from the edge of the gantry, reaching less than 700 mT at 25 cm from the edge and less than

3 mT at 250 cm from the edge as shown in Table 4. Along the x-axis, the magnetic flux densities gradually decreased while the distances away from the central axis of the scanner were increasing. The right and left symmetry was confirmed using linear regression, and the coefficient of determination ($R^2$) was 0.997. The maximum magnetic flux density value at the height of 0 cm was 680 mT or 0.68 T, at the position 25 cm away from the gantry entrance, along the center line of the z axis.

The distribution of the magnetic flux density values at the height of 50 cm (patient height level) showed the same tendency as the distribution of the magnetic flux density values at the height of 0 cm. The right and left symmetry was confirmed using linear regression, and the coefficient of determination (R2) was 0.991. The maximum measured magnetic flux density value at the height of 50 cm was 326 mT or 0.33 T, at the exact position of the maximum value at the peak of 0 cm.

Along the x-axis, at a distance 25 and 50 cm away from the gantry entrance, the magnetic flux density values at 0 cm (patient table level) were highest, followed by the values at 50 and -100 cm height, respectively. Moreover, the magnetic flux density values along the z-axis at a distance of 25 cm were higher than the values at a distance of 50 cm for all three measuring heights.

**1.2 Magnetic flux density along the gantry centerline, inside and outside of the gantry**

The result of the measured magnetic flux density, the calculated spatial gradient, and the calculated product of the magnetic flux density and the spatial gradient along the gantry centerline were showed in Fig.7 and Table 6.

From the line graph representing the magnetic flux density in Fig.7, the values inside the gantry were continuously uniform at 3 Tesla from the isocenter of the gantry to the distance 30 cm away from

the isocenter, that is, 70 cm from the gantry entrance into the gantry. Around the edge of the gantry, the magnetic flux densities decreased rapidly. The values at the gantry entrance were between 1 to 1.5 T. From the gantry entrance to the outside of the scanner along the gantry centerline, the magnetic flux densities were still decreasing and remaining less than 0.1 Tesla at a distance 80 cm away from the scanner, that is, around 290 cm from the wall near the main door of the MRI room. Consequently, along the gantry centerline, the magnetic flux density was 0.7 mT or 7 Gauss at the wall near the main entrance of the MRI room.

The spatial gradient and the product of the magnetic flux density and the spatial gradient values along the gantry centerline showed the same tendency. The values rapidly increased from around 30 cm from the isocenter and reached the maximum values at about 14 cm from the gantry entrance; after that, the spatial gradient and the product values decreased rapidly until the distance was about 50 cm away from the gantry entrance.

**2) Displacement force**

**2.1 Displacement force outside the scanner in the MRI room**

The bar charts and the tables representing the distribution of the displacement forces outside the scanner at the three heights, including -100 cm (ground level), 0 cm (patient table level), and 50 cm (patient height level), were shown in Fig.8 to 9 and Table 7 to 9.

At the height of -100 cm (ground level), the table base was fixed on the floor; therefore, some points in this area could not be measured. The displacement forces at the height of -100 cm (Fig.8,

Table 7) in the areas surrounding the table base rapidly decreased along the z and x axes. The maximum displacement force at the height of -100 cm was 0.07 N.

The displacement forces at the height 0 cm (patient table level) (Fig.9, Table 8) were decreasing while the distances along the z axis, away from the scanner, were increasing. Especially for along the 3 lines in z axis, including the central axis line and the other two lines 25 cm away from the central axis on the right and left sides, the displacement forces were rapidly decreasing from the distance 25 cm to 50 cm away from the scanner. Along the x axis, at the distance 25 cm away from the scanner, the displacement forces were also rapidly decreased. The maximum displacement force at the height 0 cm outside the scanner is 0.15 Newton (N), at the position 25 cm away from the gantry entrance along the gantry centerline. The maximum deflection angle at the height 0 cm was 88.5 degree at the same position as the maximum force.

The distribution of the displacement forces at the height 50 cm (patient height level) (Fig.10, Table 9), showed almost the same tendency along the z axis as the forces at the height 0 cm. However, along the x axis, the displacement forces changed more gradually than the values at the height 0 cm. The maximum displacement forces at the height 50 cm were 0.05 N.

**2.2 Displacement force along the gantry centerline, inside and outside of the gantry**

The distribution of displacement forces inside and outside the gantry, along the gantry centerline, is shown in Fig.11 and Table 10.

The displacement force along the gantry centerline was zero from the isocenter of the gantry to the distance 40 cm away from the isocenter, that is, 60 cm from the gantry entrance into the gantry.

The displacement forces rapidly increased from around 50 cm from the isocenter and reached the maximum value at the edge of the gantry entrance; after that, displacement forces quickly decreased until the distance was around 50 cm away from the gantry entrance.

### 2.3 Displacement force of various materials (dental materials & household items) at the two points along the gantry centerline level, 25 and 50 cm outside the gantry entrance

The diagrams representing the displacement forces of various materials at 25 and 50 cm away from the gantry, along the gantry centerline level, are shown in Fig.12.

Among all tested dental materials, the deflection angles at the position 25 cm of two kinds of forceps, mixing spatula, medical scissors, and all tested dental burs (except for an acrylic denture polishing bur) were more significant than 90 degrees; therefore, the displacement forces of these object could not be calculated. The acrylic denture polishing bur at this position exhibited the maximum calculable displacement force of 2.97 N. At 50 cm, the deflection angles of two kinds of forceps, mixing spatula, medical scissors, and two types of dental burs were still more significant than 90 degrees. The carbide cutter bur exhibited the maximum calculable displacement force, 0.29 N, at this position. However, all tested single orthodontic and prosthodontic materials received displacement forces lower than 0.03 N and 0.01 N at 25 cm and 50 cm positions, respectively.

For household items, among all tested materials, the deflection angles at the position 25 cm of scissors, battery, double clips, and a large-sized paperclip were more significant than 90 degrees, so the displacement forces of these objects could not be calculated. At this position, one type of electrical plug exhibited the maximum calculable displacement force, that is, 1.57 N. At 50 cm, only the

deflection angle of the scissors was still more significant than 90 degrees. At this position, a battery exhibited the maximum calculable displacement force, 0.59 N.

**3) Torque**

The torque measurement result was showed in Table 11. Inside the gantry, from the isocenter of the gantry to the distance 50 cm away from the isocenter, torques remained the same for all tested materials. Among the tested household items, a hairpin exhibited the highest torque, 5.75 N·cm. Among the tested dental materials, a stainless-steel arch wire (Tru-Chrome® Preformed Natural Arches .017x.025 (RMO)) exhibited the maximum torque, 0.14 N·cm. However, other dental materials made from titanium, nickel, and niobium showed no torque.

**Statistical analysis**

All measurements were performed six times. The means and standard deviation were calculated. The displacement force applied to the paper clip was statistically compared at each point with an average of ten mN or more. The displacement force applied to the plastic bracket was statistically compared at each point with an average of one mN or more.

The displacement force at points closer to the scanner was significantly larger than the displacement force at points farther away ($p<0.01$).

## DISCUSSION

### Magnetic flux density

From result of the magnetic flux density measurement of the 3T MRI scanner outside the gantry of this study, the magnetic flux densities around the area near the gantry entrance measured at the height 0 cm (patient table level) were higher than the values at the other two heights, it might be because of the pattern of the magnetic fringe fields of the MRI magnet. Inside the scanner, the magnetic field runs through the gantry in the parallel direction to the gantry centerline, then the magnetic field spreads out around the gantry entrance and encircles the MRI magnet, creating an external fringe field outside the scanner. The areas around the gantry at the height 0 cm (patient table level) that is in the same level of the gantry centerline, contain larger number of magnetic flux lines per area than at the other two heights. Regarding the results that showed the symmetrical of the magnetic flux density, it might because of the use of the solenoid magnet coil that is surrounding around the cylindrical MRI gantry and the shimming process that is used to reduce the inhomogeneities of the magnetic field and make it more uniform by adjusting the electrical currents in these coils. Moreover, the reason that the magnetic flux density values were rapidly attenuated and decreased near the gantry entrance is might be because of the active shield magnet coils that is used to reduce the size of the external magnetic field of the high-field MRI scanner (29,30).

From the result of the magnetic flux density along the gantry centerline, inside and outside of the gantry, the magnetic flux density was very uniform inside of the gantry. However, the values were

decreasing rapidly from the area around the gantry entrance to the area outside the scanner, changing from 1.5 T to less than 0.1 T within the distance just 100 cm away from the edge of the gantry entrance. It might be because of the active shield magnet coil (mentioned previously) installed near the gantry's opening. Because of the broad change in the magnetic flux density values around the gantry entrance area, there was a considerable change in the magnetic flux densities per distance here. Therefore, from this study result, the peak values of the spatial gradient and the product of the magnetic flux density and the spatial gradient occurred within 14 cm inside the outer edge of the gantry entrance.

The fringe field map or the iso-gauss line map can represent the MRI room's magnetic field densities. Generally, the 5 Gauss (0.5 mT) line is the boundary line for the access control. Electronically powered or magnetically programmed active implanted medical devices (AIMDs), such as cardiac implanted electronic devices (CIEDs), are prohibited from entering beyond the 5 Gauss line because the risk of magnetic field-induced device malfunction that can cause harmful effects to the patient (1,29,31). Moreover, the 200 Gauss (20 mT) zone is the limit for the projectile hazard; significant displacement forces can be exerted on ferromagnetic objects entering beyond this zone (1,9,32). From the magnetic flux density outside and inside the scanner measured in this study, some part of the 5 Gauss line is located just outside the MRI room at the main door. And, at the edge of the room, the magnetic flux density ranges from 3 to 7 Gauss. Therefore, the patient with the AIMDs is prohibited from entering the MRI room. The dangerous projectile effect can occur if the ferromagnetic objects are entered beyond the distance of around 125 cm from the MRI scanner.

**Displacement force and Magnetic flux density**

Displacement forces distribution outside the scanner at the height 0 cm (patient table level) and 50 cm (patient height level) showed almost the same tendency to the magnetic flux density distribution at the same heights. However, the displacement forces at the areas near the gantry entrance were much larger than the places far away compared to the magnetic flux density distribution pattern. Because the change of the magnetic flux densities per distance or the spatial gradient of the magnetic field was more significant at the areas near the gantry, the displacement forces were also larger here. It was said that the spatial gradients are a crucial parameter determining the displacement force exerted on an object (4,33). The displacement forces measured along the gantry centerline also showed the same tendency as the measured displacement forces outside of the scanner.

Moreover, the displacement forces measured along the gantry centerline also showed the same tendency as the calculated spatial gradient and the product of the spatial gradient and the static magnetic field. For paramagnetic or unsaturated ferromagnetic material, the displacement force depends on both the static magnetic field and the spatial gradient, that is, the product of them (1,4,25). For saturated ferromagnetic material, the displacement force depends on the spatial gradient (1,4,25).

Some previous studies (34,35,36,37) studied on the displacement forces on dental materials. Still, all of them were measured at only one position, the position of the highest spatial gradient around the gantry entrance area. Except for one study, Omatsu et al. (38) measured the displacement forces of one type of dental keeper by varying the positions along the z-axis. The maximum force occurred within 10 cm inside the scanner's gantry for both 1.5T and 3T scanners.

The distribution pattern of the displacement force at -100 cm (ground level) differed from the magnetic flux density. It might be because of the presence of the table base.

Regarding the result of displacement force at two positions along the gantry centerline, at 25 and 50cm, almost all tested household items exhibited deflection angles more significant than 45 degrees at both positions. Among tested dental materials, all materials made from stainless steel showed a deflection angle more significant than 45 degrees at both two positions, except for only some stainless-steel materials, such as the plastic bracket, which contains a small piece of wire inside, and the molar band had a deflection angle lower than 45 degrees. The ASTM F2052-15 (25) indicated that if the device deflects less than 45 degrees, the displacement force is less than the force on the device due to gravity (its weight). For this condition, it is assumed that any risk imposed by applying the magnetically induced force is no longer than any risk imposed by regular daily activity in the Earth's gravitational field. For forces more significant than gravity, the location of the implant and means of fixation must be considered. Almost all household items made from stainless steel had a deflection angle of more than 90 degrees near the gantry entrance. Therefore, the displacement forces of these materials were huge around here. However, their deflection angles and displacement forces could not be measured and calculated because a tangent of 90 degrees is equal to infinity. The displacement forces on all tested dental materials used in the oral cavity were 50 to 100 times lower than the calculable (measurable) displacement forces on stainless steel household items and dental material used outside the oral cavity.

The displacement forces also depend on the materials' magnetic susceptibility (1,2,4). It was noticed from this study result that the deflection angles and displacement forces on household items and some dental materials used outside the oral cavity made from stainless steel (or contain stainless steel component) were considerably more significant than the displacement forces on the dental materials used inside the oral cavity made from stainless steel. The reason is that the kinds of stainless steel are different, so the magnetic susceptibility is also different. There are three main kinds of stainless steel, including

austenitic stainless steel (AISI 300 series), which is paramagnetic; ferritic stainless steel, which is ferromagnetic; and martensitic stainless steel (AISI 400 series), which is also ferromagnetic (39,40,41). Dental and medical devices and materials used inside the oral cavity or human body, such as orthodontic arch wires, brackets, and medical implants, are usually made from austenitic stainless steel (25,40-44). However, some medical devices, such as surgical instruments, and household items in everyday life are usually made from ferritic or martensitic stainless steel (25,40-44). Moreover, the displacement force also depends on the volume of the material (1,4,25), it was said that the ratio of the displacement force to the gravity force (or weight of material) will prove useful in estimating the degree to which an MRI magnetic field can pull on object (4). From this study result, At the position 50 cm, the force ratios between displacement force and the material weight of a medium-sized double clip (household item) and a stainless-steel bracket (dental material) were 7.15 and 1.33 respectively, that is the double clip was affected 5.4 times more than the stainless-steel bracket. A prosthetic magnet keeper composing of iron, that is ferromagnetic, also showed the same result as the stainless-steel bracket. On the contrary, tested dental materials such as Nickel-Titanium orthodontic arch wire and

extension spring, Maxillary quad helix composing of Elgiloy® (Co-Cr-Ni-Mo alloy), bridge framework containing Au-Ag-Pd alloy, and Co-Cr denture clap exhibited no displacement forces. Although pure form Ni and Co are ferromagnetic, Elgiloy® (Co-Cr-Ni-Mo alloy) is paramagnetic in nature (45). There are also evidences that Co-Cr alloy is non-magnetic (46,47).

Because the deflection angles, measured in our preliminary test, of the tested keeper and the stainless-steel arch wires were more than 90 degrees at the gantry entrance, the true maximum forces could not be calculated. This study measured at the position 25 cm away from the gantry entrance instead. The deflection angles of them were the same at 82 degrees and the displacement forces was 0.005 N for the keeper and were 0.03 N for two tested arch wires. Omatsu et al. (38) has measured the displacement force of a keeper (4mm in diameter) and found that the calculated maximum force on the keeper from their study was much considerably lesser than the adhesive force (120 N) that was converted from the tensile bond strength (MPa) measured from the study of Hashimoto et al. (48). Klock et al. (24) mentioned that a total force of under 1 N on fixed orthodontic appliance per arch is within the range of orthodontic forces and should not result in displacement of adequately-ligated appliance parts. However, the possibility of discomfort similar to that caused by orthodontic appliance activation should be informed to the patient before to the MRI examination.

**Torque**

From this study result, hairpin made from steel and stainless-steel paperclip that were ferromagnetic exhibited considerably larger torque comparing to all tested stainless steel arch wires that were paramagnetic and exhibited smaller torque, that is equal to or less than 0.1 N·cm. Moreover,

torque remained the same within the distance of 50 cm from the isocenter. The above results support the theory that torque depends on the material's shape, the magnetic susceptibility, and the static magnetic field (1,4,5). The tendency of measured torque was by the measured magnetic flux density values that were uniform at 3T inside the gantry. The torque depends directly on the strength of the magnetic field, and therefore at its maximum at the isocenter of the MRI scanner (1,36,49).

Almost all of the selected tested material had elongated shape because the theory that the significant torque will occur to asymmetric shape objects, such as cylinders or ellipsoids (1,4).

Additionally, only tested material made from steel and stainless-steel exhibited torque because torque is also depending on the magnetic property of the material (1,4).

**Study limitations**

It was impossible to measure the displacement forces in all targeted materials at various positions along the gantry centerline because some tested materials showed the deflection angles more than 90 degrees near the gantry entrance. In future study, the appropriate and effective methods for measurement of the displacement forces of these materials at various positions inside the gantry should be investigated. For example, addition of non-magnetic weight to the thread in order to decrease the deflection angle of the tested material or measurement of the displacement force directly by the force gauge that made from non-magnetic materials.

## CONCLUSION

The magnetic flux density outside the gantry was greatest and bilaterally symmetrical at the height of the patient table. It decreased with increasing distance from the edge of the gantry, reaching less than 700 mT at 25 cm from the edge and less than 3 mT at 250 cm from the edge. The magnetic flux density inside the scanner was uniform at 3T at the isocenter area.

The magnetically induced displacement force related to the spatial gradient of magnetic field and the product of magnetic flux density and the spatial gradient. The greatest displacement force occurred at the gantry entrance. However, there was no displacement force around the isocenter of the gantry because the spatial gradient of magnetic field was zero there. For the MRI examination, the effect of displacement force is strongest at the gantry entrance, where the patient passed in or out of the scanner. On the other hand, the effect of torque is greatest around the isocenter of the gantry, during the MRI examination.

Inadequately or poorly fixed intraoral stainless steel dental orthodontic and prosthodontic appliances could be dislodged due to the displacement force. And, effect of torque was small enough to be of no concern for dental metals. The status of the fixation of all intraoral dental metals has to be confirmed before and after the MRI examination.

**REFERENCES**


1. Stafford RJ. The Physics of Magnetic Resonance Imaging Safety. *Magn Reson Imaging Clin N Am*. 2020;28(4):517-536.
2. Sammet S. Magnetic resonance safety. *Abdom Radiol (NY)*. 2016;41(3):444-451.
3. Felemban D, Verdonschot RG, Iwamoto Y, et al. A quantitative experimental phantom study on MRI image uniformity. *Dentomaxillofac Radiol*. 2018;47(6):20180077.
4. Panych LP, Madore B. The physics of MRI safety. *J Magn Reson Imaging*. 2018;47(1): 28-43.
5. Kanal E. Standardized Approaches to MR Safety Assessment of Patients with Implanted Devices. *Magn Reson Imaging Clin N Am*. 2020;28(4):537-548.
6. Sfondrini MF, Preda L, Calliada F, et al. Magnetic Resonance Imaging and Its Effects on Metallic Brackets and Wires: Does It Alter the Temperature and Bonding Efficacy of Orthodontic Devices?. *Materials (Basel)*. 2019;12(23):3971.
7. Kuroda K, Yatsushiro S. New Insights into MR Safety for Implantable Medical Devices. *Magn Reson Med Sci*. 2022;21(1):110-131.
8. Ayyıldız S, Kamburoğlu K, Sipahi C, Murat S, Görgülü S, Pişkin B. Radiofrequency heating and magnetic field interactions of fixed partial dentures du ring 3-tesla magnetic resonance imaging. *Oral Surg Oral Med Oral Pathol Oral Radiol*. 2013;116(5):640-647.
9. U.S. Food and Drug Administration. Guidance for industry and Food and Drug Administration staff: Testing and labeling medical devices for safety in the magnetic Resonance (MR) environment. https://www.fda.gov/regulatory-information/search-fda-

guidance-documents/testing-and-labeling-medical-devices-safety-magnetic-resonance-mr-environment. Published May 20, 2021.

10. Elison JM, Leggitt VL, Thomson M, Oyoyo U, Wycliffe ND. Influence of common orthodontic appliances on the diagnostic quality of cranial magnetic resonance images. *Am J Orthod Dentofacial Orthop*. 2008;134(4):563-572.
11. Görgülü S, Ayyildiz S, Kamburoglu K, Gökçe S, Ozen T. Effect of orthodontic brackets and different wires on radiofrequency heating and magnetic field interactions during 3-T MRI. *Dentomaxillofac Radiol*. 2014;43(2):20130356.
12. Hubálková H, La Serna P, Linetskiy I, Dostálová T. Dental alloys and magnetic resonance imaging. *Int Dent J*. 2006;56(3):135-141.
13. Mathew CA, Maller S, Maheshwaran. Interactions between magnetic resonance imaging and dental material. *J Pharm Bioallied Sci*. 2013;5(Suppl 1):S113- S116.
14. Shellock FG, Woods TO, Crues JV 3rd. MR labeling information for implants and devices: explanation of terminology. *Radiology*. 2009;253(1):26-30.
15. Shellock FG, Crues JV 3rd. MR safety and the American College of Radiology White Paper. *AJR Am J Roentgenol*. 2002;178(6):1349 –1352.
16. Destine D, Mizutani H, Igarashi Y. Metallic artifacts in MRI caused by dental alloys and magnetic keeper. *Nihon Hotetsu Shika Gakkai Zasshi*. 2008;52:205-210.
17. Rao J, Shah A, Singh K, Tiwari B. Prosthetic and dental implant patient's biosafety during MRI procedure: A survey based study on awareness among professionals. *J Interdiscip Dentistry*. 2022;12(2):47-52.

18. Shafiei F, Honda E, Takahashi H, Sasaki T. Artifacts from dental casting alloys in magnetic resonance imaging. *J Dent Res*. 2003;82:602-606.

19. Tran LTX, Sakamoto J, Kuribayashi A, Watanabe H, Tomisato H, Kurabayashi T. Quantitative evaluation of artefact reduction from metallic dental materials in short tau inversion recovery imaging: efficacy of syngo WARP at 3.0 tesla. *Dentomaxillofac Radiol*. 2019;48(7):20190036.

20. Hasegawa M, Miyata K, Abe Y, Ishigami T. Radiofrequency heating of metallic dental devices during 3.0 T MRI. *Dentomaxillofac Radiol*. 2013;42(5):20120234.

21. Ruf S, Pancherz H. Temporomandibular joint remodeling in adolescents and young adults during Herbst treatment: A prospective longitudinal magnetic resonance imaging and cephalometric radiographic investigation. *Am J Orthod Dentofacial Orthop*. 1999;115(6):607-618.

22. Dobai A, Dembrovszky F, Vízkelety T, Barsi P, Juhász F, Dobó-Nagy C. MRI compatibility of orthodontic brackets and wires: systematic review article. *BMC Oral Health*. 2022;22(1):298.

23. Klocke A, Kemper J, Schulze D, Adam G, Kahl-Nieke B. Magnetic field interactions of orthodontic wires during magnetic resonance imaging (MRI) at 1.5 Tesla. *J Orofac Orthop*. 2005;66(4):279-287.

24. Klocke A, Kahl-Nieke B, Adam G, Kemper J. Magnetic forces on orthodontic wires in high field magnetic resonance imaging (MRI) at 3 tesla. *J Orofac Orthop*. 2006;67(6):424-429.

25. American Society for Testing and Materials International. *Designation: ASTM F2052-15, standard test method for measurement of magnetically induced displacement force on medical devices in the magnetic resonance environment*. West Conshohocken, Pa: American Society for Testing and Materials International; 2015.

26. Schenck JF. The role of magnetic susceptibility in magnetic resonance imaging: MRI magnetic compatibility of the first and second kinds. *Med Phys*. 1996;23(6):815-850.

27. American Society for Testing and Materials International. *Designation: ASTM F2213-17, standard test method for measurement of magnetically induced torque on medical devices in the magnetic resonance environment*. West Conshohocken, Pa: American Society for Testing and Materials International; 2017.

28. Mcrobbie D. *Essentials of MRI Safety*. Hoboken NJ: Wiley Blackwell; 2020.

29. Turner BD. Shielding issues for medical products. *Conformity*. 2007;48-53.

30. Westbrook C, Talbot J. *Mri in Practice*. Fifth ed. Hoboken NJ: Wiley Blackwell; 2019: 346-369.

31. U.S. Food and Drug Administration. Guidance for industry and Food and Drug Administration staff: Submission of premarket notifications for magnetic resonance diagnostic devices. https://www.fda.gov/regulatory-information/search-fda-guidance-documents/submission-premarket-notifications-magnetic-resonance-diagnostic-devices. Published November 18, 2016.

32. Greenberg KL, Weinreb J, Shellock FG. "MR conditional" respiratory ventilator system incident in a 3-T MRI environment. *Magn Reson Imaging*. 2011;29(8):1150-1154.

33. Panych LP, Kimbrell VK, Mukundan S Jr, Madore B. Relative Magnetic Force Measures and Their Potential Role in MRI Safety Practice. *J Magn Reson Imaging*. 2020;51(4):1260-1271.

34. Miyata K, Hasegawa M, Abe Y, Tabuchi T, Namiki T, Ishigami T. Radiofrequency heating and magnetically induced displacement of dental magnetic attachments during 3.0 T MRI. *Dentomaxillofac Radiol*. 2012;41(8):668-674.

35. Görgülü S, Ayyildiz S, Kamburoglu K, Gökçe S, Ozen T. Effect of orthodontic brackets and different wires on radiofrequency heating and magnetic field interactions during 3-T MRI. *Dentomaxillofac Radiol*. 2014;43(2):20130356.

36. Kemper J, Priest AN, Schulze D, Kahl-Nieke B, Adam G, Klocke A. Orthodontic springs and auxiliary appliances: assessment of magnetic field interactions associated with 1.5 T and 3 T magnetic resonance systems. *Eur Radiol*. 2007;17(2):533-540.

37. Hasegawa M, Miyata K, Abe Y, Ishii T, Ishigami T, Ohtani K, Nagai E, Ohyama T, Umekawa Y, Nakabayashi S. 3-T MRI safety assessments of magnetic dental attachments and castable magnetic alloys. *Dentomaxillofac Radiol*. 2015;44(6):20150011.

38. Omatsu M, Obata T, Minowa K, Yokosawa K, Inagaki E, Ishizaka K, Shibayama K, Yamamoto T. Magnetic displacement force and torque on dental keepers in the static magnetic field of an MR scanner. *J Magn Reson Imaging*. 2014;40(6):1481-1486.

39. Woods TO, Delfino JG, Jana, Rajan S. Assessment of Magnetically Induced Displacement Force and Torque on Metal Alloys Used in Medical Devices. *J Test Eval*. 2021;49(2): 783-795.

40. Woods TO. MRI Safety and Compatibility of Implants and Medical Devices. In: Winters G, Nutt M, ed. *Stainless Steels for Medical and Surgical Applications*. West Conshohocken, Pa: American Society for Testing and Materials International; 2003.82–90.

41. Arango S, Ossa C. Stainless Steel: Material Facts for the Orthodontic Practitioner. *Revista Nacional de Odontología*. 2015;11(20).73-82.

42. Oh KT, Choo SU, Kim KM, Kim KN. A stainless steel bracket for orthodontic application. *Eur J Orthod*. 2005;27(3):237-244.

43. Festas A, Ramos A, Davim J. Medical devices biomaterials – A review. *Proceedings of the Institution of Mechanical Engineers, Part L: Journal of Materials: Design and Applications*. 2020;234(1):218-228.

44. Niinomi M. Metallic biomaterials. *J Artif Organs*. 2008;11(3):105-110.

45. Ho JC, Shellock FG. Magnetic properties of Ni-Co-Cr-base Elgiloy. *J Mater Sci Mater Med*. 1999;10(9):555-560.

46. Al Jabbari YS. Physico-mechanical properties and prosthodontic applications of Co-Cr dental alloys: a review of the literature. *J Adv Prosthodont*. 2014;6(2):138-145.

47. Starcuková J, Starcuk Z Jr, Hubálková H, Linetskiy I. Magnetic susceptibility and electrical conductivity of metallic dental materials and their impact on MR imaging artifacts. *Dent Mater*. 2008;24(6):715-723.

48. Hashimoto M, Ohno H, Koga M, Endo K, Sano H, Oguchi H. In vivo degradation of resin-dentin bonds in humans over 1 to 3 years. *J Dent Res*. 2000;79:1385–1391.

49. Eerkens HJ, Smits C, Hofman MBM. Cochlear Implant Magnet Dislocation: Simulations and Measurements of Force and Torque at 1.5T Magnetic Resonance Imaging. *Ear Hear*. 2021;42(5):1276-1283.

**ACKNOWLEDGMENTS**

I would like to express my sincere appreciation to Professor Shumei Murakami who kindly accepted me as a Ph.D. student at the department of Oral and Maxillofacial Radiology and his precious suggestion, support and endless encouragements to make this thesis possible.

I would like to express my deep gratitude to Assistant Professor Yuka Uchiyama, whose kindly support and encouragements through the research period and my study life in Japan.

I am deeply thankful to all staff and colleagues at our department for their help and support.

Many thanks to Srinakharinwirot University, Thailand, to grant me the scholarship and support my living in Japan.

## FIGURE LEGENDS

**Figure 1.** Measured points at intersections of two lines

The measured points for the magnetic flux density and displacement force outside the scanner were two-dimensionally 25 cm grid intersection, at three of the heights, namely -100 cm (ground level), 0 cm (patient table level), and 50 cm (patient height level). All measured points were located along the three axes (x, y, z).

**Figure 2.** Apparatus for measuring of deflection angle and the illustration of deflection angle measurement method

Two threads are tied from the center of the protractor. One thread is attached to the reference lead, and the other thread is attached to the tested material (orthodontic bracket in this photo). The angle formed by the two threads was read in tenths of a degree.

**Figure 3.** Apparatus for measuring of torque and the illustration of measurement method

A pulley-based torque measuring instrument was constructed according to ASTM recommendations. The tested material's long axis is parallel to the magnetic field. The torque was calculated from the weight when the tested material made an angle of 45 degrees with the magnetic field.

**Figure 4.** Magnetic flux density (mT) at y=-100 cm (ground level)

On the ground level, the magnetic flux density was measured at 350 cm in the z-axis direction (15 places) and 200 cm in the x-axis direction (9 places) at intervals of 25 cm. Since the measuring instrument has high directivity, the maximum value was taken as the measured value while rotating it 180 degrees. Due to the table base, measuring at the center of the z=25cm point was impossible. Except for these points, the magnetic flux density was symmetrical in the right-left direction. When the z-axis coordinate exceeded 75 cm, the magnetic flux density was below 10 mT.

**Figure 5.** Magnetic flux density (mT) at y=0 cm (patient table level)

On the patient table level, the magnetic flux density was measured at 350 cm in the z-axis direction (15 places) and 200 cm in the x-axis direction (9 places) at intervals of 25 cm. Since the measuring instrument has high directivity, the maximum value was taken as the measured value while rotating it 180 degrees. The magnetic flux density was symmetrical in the right-left direction. When the z-axis coordinate exceeded 175 cm, the magnetic flux density was below 10 mT.

**Figure 6.** Magnetic flux density (mT) at y=50 cm (patient height level)

On the patient height level, the magnetic flux density was measured at 350 cm in the z-axis direction (15 places) and 200 cm in the x-axis direction (9 places) at intervals of 25 cm. Since the measuring instrument has high directivity, the maximum value was taken as the measured value while rotating it 180 degrees. The magnetic flux density was symmetrical in the right-left direction. When the z-axis coordinate exceeded 175 cm, the magnetic flux density was below 10 mT.

**Figure 7.** B, dB/dz, and their product

The magnetic flux density along the gantry centerline, inside and outside the gantry, was measured by placing of the measuring probe on the patient bed and the patient bed was moved in and out of the gantry. The magnetic flux density inside the gantry was uniform at 3 T within 30 cm away from the isocenter of the gantry. Then the values were decreasing rapidly around the gantry entrance. The tendency of the spatial gradient of magnetic field (dB/dz) and the product of the static magnetic field (or the magnetic flux density at each position) (B) and dB/dz was almost the same, the value was zero around the isocenter area and then rapidly increasing to the maximum at around the distance 0 to -15 cm from the gantry entrance. The maximum measurable dB/dz and the product dB/dz and B of were 4.8 T/m and 9.7 $T^2$/m, respectively. After that, the magnetic flux density was decreasing rapidly from the gantry entrance to outside of the scanner.

**Figure 8.** Displacement force (N) at y=-100 cm (ground level)

On the patient ground level, the deflection angle was measured at 350 cm in the z-axis direction (15 places) and 200 cm in the x-axis direction (9 places) at intervals of 25 cm. Then, the displacement force was calculated from the measured deflection angle and the material's weight. Due to the table base, measuring at the center of the z=25cm point was impossible. Except for these points, the displacement forces outside the gantry at ground level decreased rapidly from the areas near the gantry to the farther distances along the x and z-axes. When the z-axis coordinate exceeded 100 cm, the displacement force was below 0.01 N.

**Figure 9.** Displacement force (N) at y=0 cm (patient table level)

At the patient table level, the deflection angle was measured at 350 cm in the z-axis direction (15 places) and 200 cm in the x-axis direction (9 places) at intervals of 25 cm. Then, the displacement force was calculated from the measured deflection angle and the material's weight. The displacement forces outside the gantry at patient table level decreased rapidly from the areas near the gantry to the farther distances along the x and z-axes. When the z-axis coordinate exceeded 100 cm, the displacement force was below 0.01 N.

**Figure 10.** Displacement force (N) at y=50 cm (patient height level)

At the patient height level, the deflection angle was measured at 350 cm in the z-axis direction (15 places) and 200 cm in the x-axis direction (9 places) at intervals of 25 cm. Then, the displacement force was calculated from the measured deflection angle and the material's weight. The displacement forces outside the gantry at patient height level decreased rapidly from the areas near the gantry to the farer distances along the x and z-axes. When the z-axis coordinate exceeded 75 cm, the displacement force was below 0.01 N.

**Figure 11.** Displacement force along gantry center (mN)

The displacement force was measured along the patient bed at every 5 cm along z axis. The displacement force along the gantry centerline was zero from the isocenter of the gantry to the distance 40 cm away from the isocenter. The displacement forces rapidly increased from around 50 cm from the isocenter and reached the maximum value at the gantry entrance; after that, displacement forces

quickly decreased until the distance was around 50 cm away from the gantry entrance. The distribution of the displacement force along the gantry centerline showed almost the same tendency to the dB/dz and the product of dB/dz and B.

**Figure 12.** Displacement force on materials (N) at z= 25 and 50 cm

The displacement forces of all tested 44 materials at the 2 positions, 25 cm and 50 cm along the z-axis. Stainless steel extraoral dental devices exhibited considerable larger displacement forces than stainless steel intraoral dental materials. At the position 25 and 50 cm, some of the dental materials and household items exhibited the deflection angles more than 90 degrees, so their displacement forces could not be calculated. At the position 25 cm, the acrylic denture polishing bur showed the maximum calculable displacement force of 2.97 N and one type of electrical plug exhibited the maximum calculable displacement force, that is, 1.57 N. At the position 50 cm, the carbide cutter bur exhibited the maximum calculable displacement force, 0.29 N. an AAA battery exhibited the maximum calculable displacement force, 0.59 N. However, all tested single orthodontic and prosthodontic materials received displacement forces lower than 0.03 N and 0.01 N at 25 cm and 50 cm positions, respectively.

## TABLE LEGENDS

**Table 1.** Tested materials for displacement force measuremenent

The total number of tested materials is 44, including both dental materials and household items.

**Table 2.** Tested materials for torque measuremenent

The total number of tested materials is 14, including both dental materials and household items.

**Table 3.** Magnetic flux density (mT) at y=-100 cm (ground level)

On the ground level, the magnetic flux density was measured at 350 cm in the z-axis direction (15 places) and 200 cm in the x-axis direction (9 places) at intervals of 25 cm. Since the measuring instrument has high directivity, the maximum value was taken as the measured value while rotating it 180 degrees. Due to the table base, measuring at the center of the z=25cm point was impossible. The maximum measurable magnetic flux density value was 60 mT at the position x=50 cm and z=25 cm.

**Table 4.** Magnetic flux density (mT) at y=0 cm (patient table level)

On the patient table level, the magnetic flux density was measured at 350 cm in the z-axis direction (15 places) and 200 cm in the x-axis direction (9 places) at intervals of 25 cm. Since the measuring instrument has high directivity, the maximum value was taken as the measured value while rotating it 180 degrees. At the patient table level, the maximum magnetic flux density value was 680 mT at the position x=0 cm (the gantry centerline) and z=25 cm.

**Table 5.** Magnetic flux density (mT) at y=50 cm (patient height level)

On the patient height level, the magnetic flux density was measured at 350 cm in the z-axis direction (15 places) and 200 cm in the x-axis direction (9 places) at intervals of 25 cm. Since the measuring instrument has high directivity, the maximum value was taken as the measured value while rotating it 180 degrees. At the patient height level, the maximum measurable magnetic flux density value was 326 mT at the position x=0 cm (the gantry centerline) and z=25 cm.

**Table 6.** Magnetic flux density along gantry centeline, and dB/dz, and their product

The magnetic flux density along the gantry centerline, inside and outside the gantry, was measured by placing of the measuring probe on the patient bed and the patient bed was moved in and out of the gantry.

The magnetic flux density (B) was uniform and highest at 3 T around the isocenter area inside the gantry. The spatial gradient (dB/dz) and the product of dB/dz and B was highest around the gantry entrance. The maximum measurable dB/dz and the product dB/dz and B of were 4.8 T/m and 9.7 $T^2$/m, respectively.

**Table 7.** Displacement force (mN) at y=-100 cm (ground level)

On the ground level, the deflection angle was measured at 350 cm in the z-axis direction (15 places) and 200 cm in the x-axis direction (9 places) at intervals of 25 cm. Then, the displacement force was calculated from the measured deflection angle and the material's weight. Due to the table base, measuring at the center of the z=25cm point was impossible. The measurable maximum

displacement force at the ground level was 65.7 mN at the position x=25 cm (the gantry centerline) and z=50 cm.

**Table 8.** Displacement force (mN) at y=0 cm (patient table level)

On the patient table level, the deflection angle was measured at 350 cm in the z-axis direction (15 places) and 200 cm in the x-axis direction (9 places) at intervals of 25 cm. Then, the displacement force was calculated from the measured deflection angle and the material's weight. The maximum displacement force outside the gantry at the patient table level was 151.8 mN at the position x=0 cm (the gantry centerline) and z=25 cm.

**Table 9.** Displacement force (mN) at y=50 cm (patient height level)

On the patient height level, the deflection angle was measured at 350 cm in the z-axis direction (15 places) and 200 cm in the x-axis direction (9 places) at intervals of 25 cm. Then, the displacement force was calculated from the measured deflection angle and the material's weight. The maximum displacement force outside the gantry at the patient height level was 52.3 mN at the position x=0 cm (gantry centerline) and z=25 cm.

**Table 10.** Deflection angle (degree) and Displacement force (mN) along gantry centerline

The displacement force was measured along the patient bed at every 5 cm along z axis. The maximum measured deflection angle and the maximum displacement force along the gantry centerline was at the position x=0 and z=0 cm (the gantry entrance). For the representative tested material, the

maximum deflection angle and displacement force were 62.85 degrees and 2.1 mN, respectively. However, it is possible that the more precise displacement force will occur between the distance z=0 cm (gantry entrance) and z=-5 cm, inside the gantry entrance.

**Table 11.** Torque (N·cm)

The measurement of torque was performed at 6 positions inside the gantry, including at the isocenter of the gantry (0), 10, 20, 30, 40, and 50 cm along the gantry centerline level.

Inside the gantry, tested steel household items exhibited dramatically larger torques than the stainless-steel intraoral dental materials. Among all tested household items, hairpin made from steel exhibited greatest torque that is 5.8 N·cm. Among all tested dental materials, five of tested stainless steel orthodontic arch wires (from all tested seven different stainless steel arch wires) showed the highest torque that is 0.1 N·cm. Tested dental materials containing Ti-Nb alloy, Ni-Ti alloy, and Co-Cr-Ni-Mo alloy exhibited no torque.

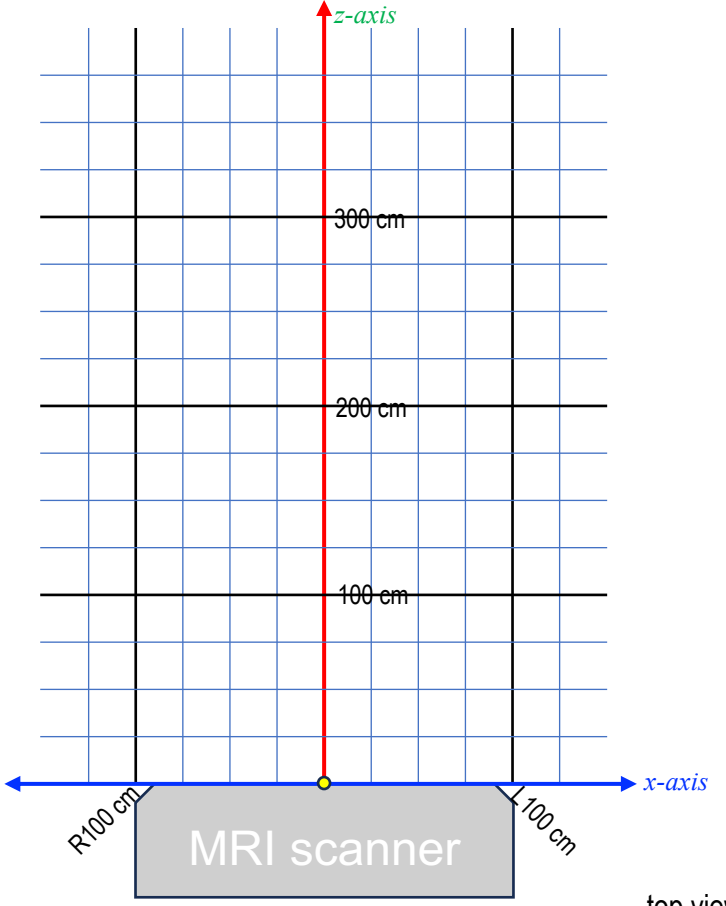


top view

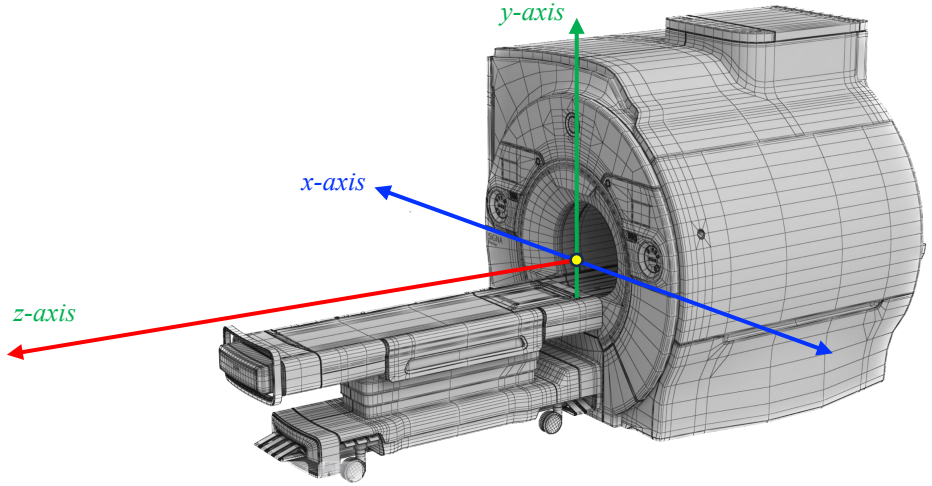


3D view

front view

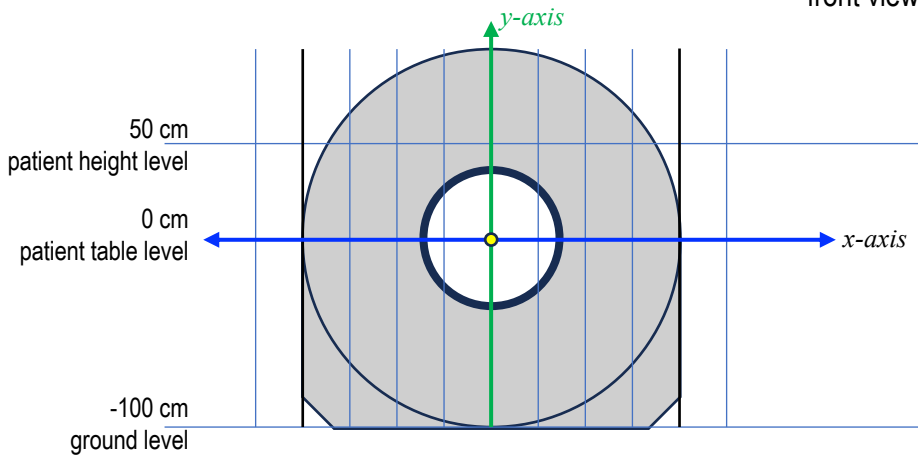


lateral view

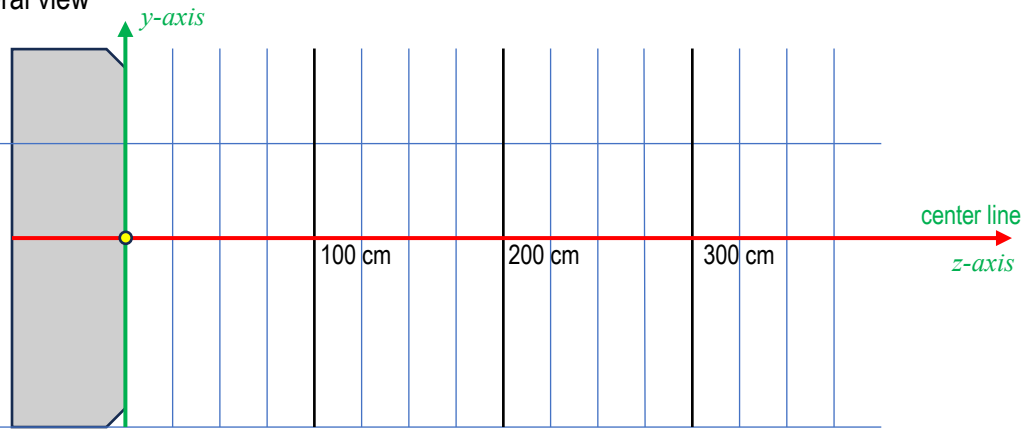


Figure 1. Measured points at intersections of two lines

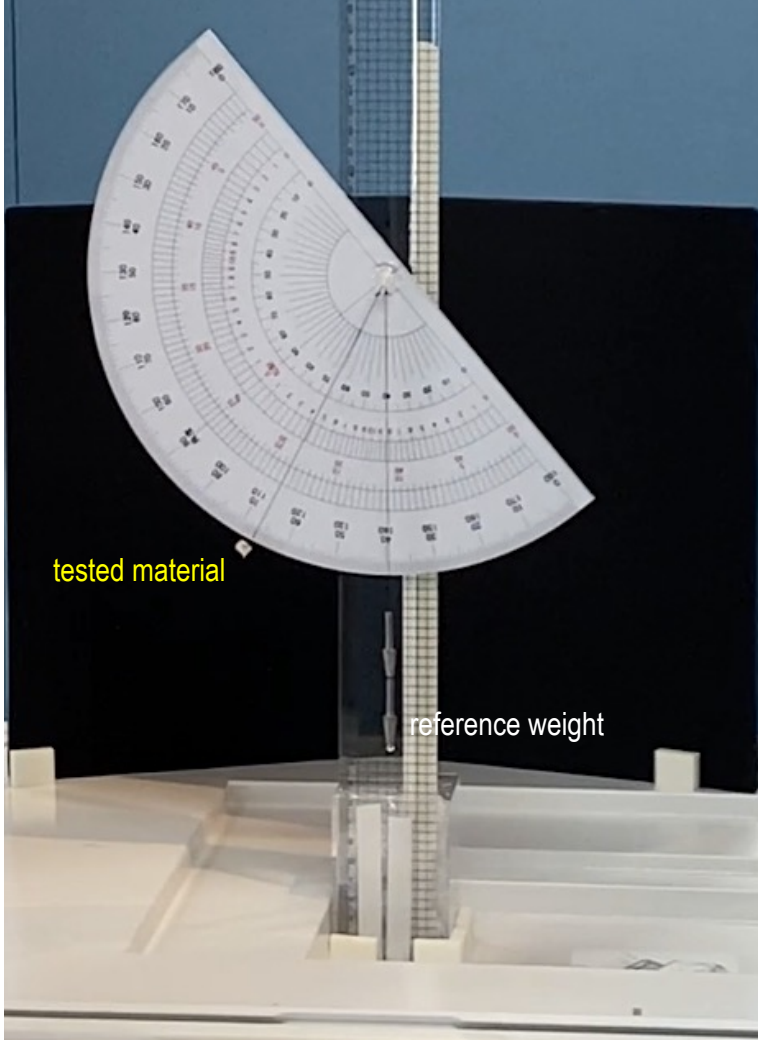


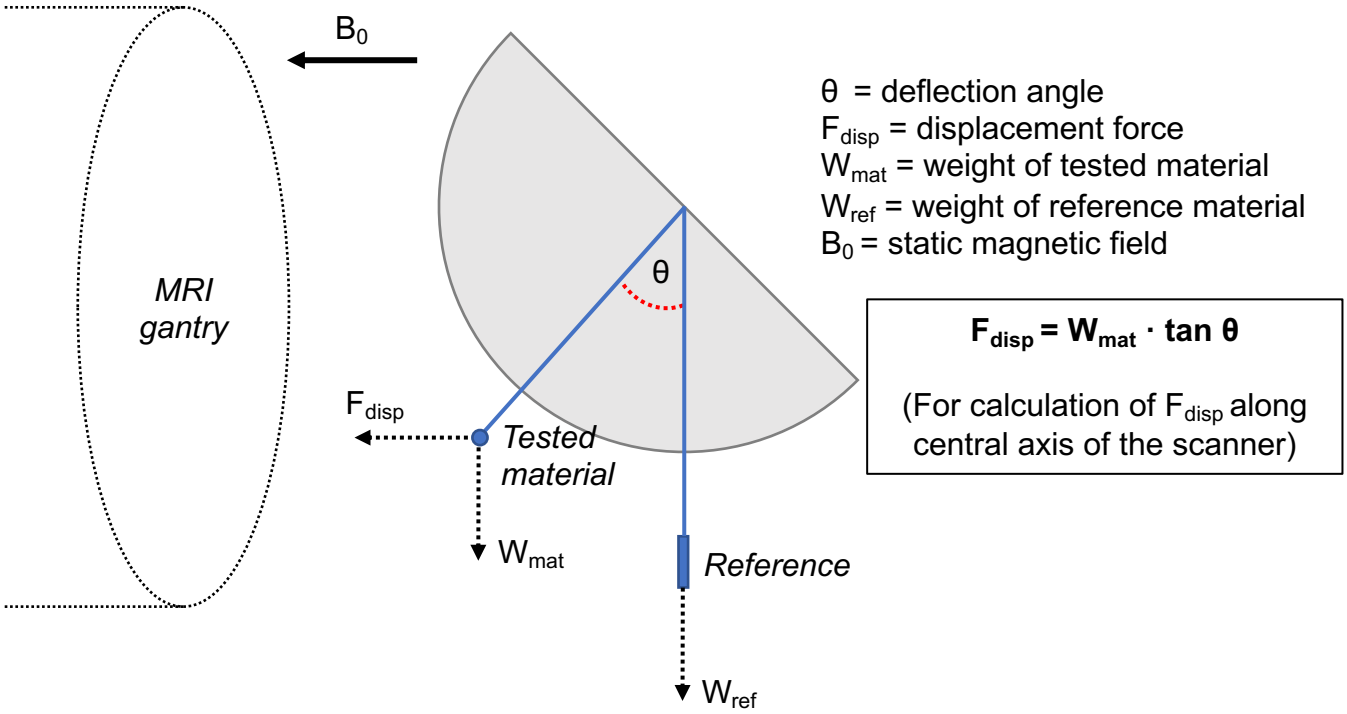


Figure 2. Apparatus for measuring of deflection angle and the illustration of deflection angle measurement method

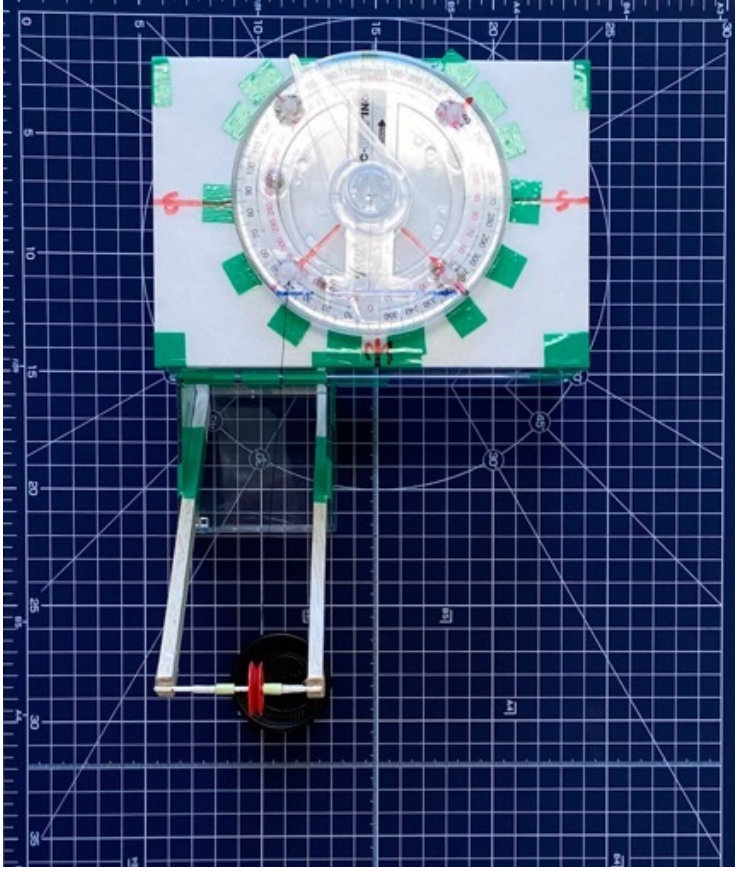

*Top view*

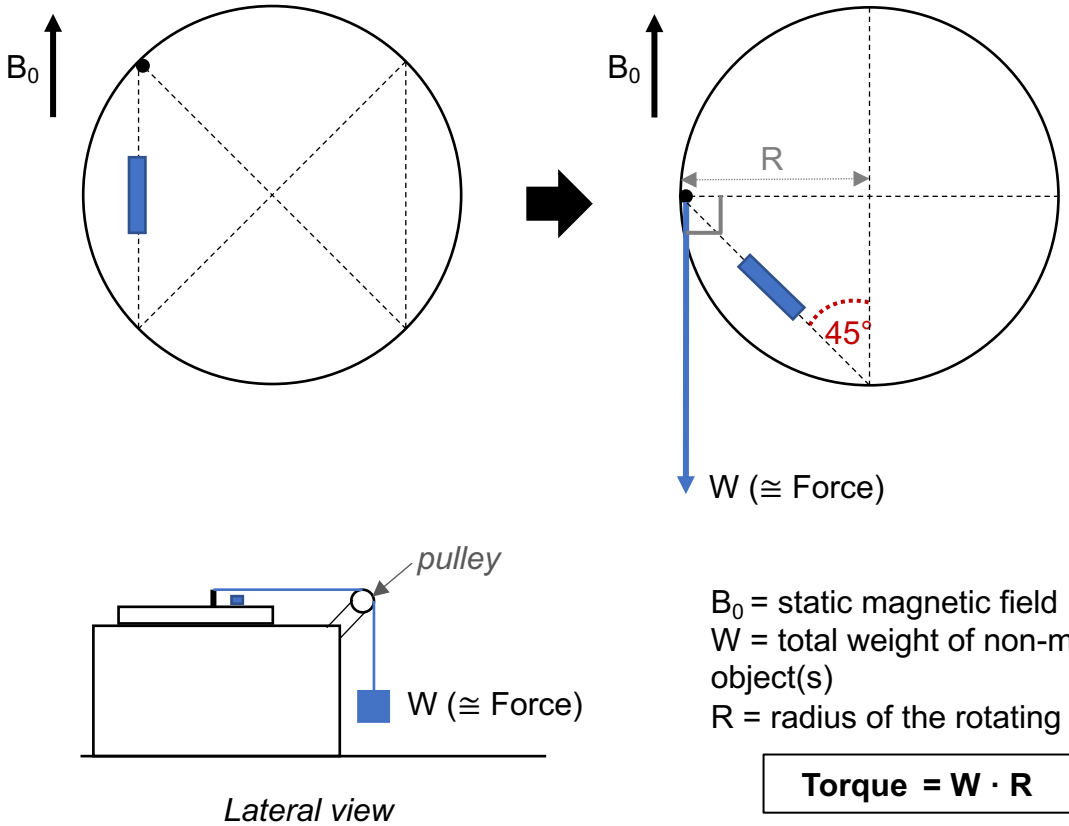


*Lateral view*

$B_0$ = static magnetic field
W = total weight of non-magnetic object(s)
R = radius of the rotating plate

**Torque = W · R**

Figure 3. Apparatus for measuring of torque and the illustration of measurement method

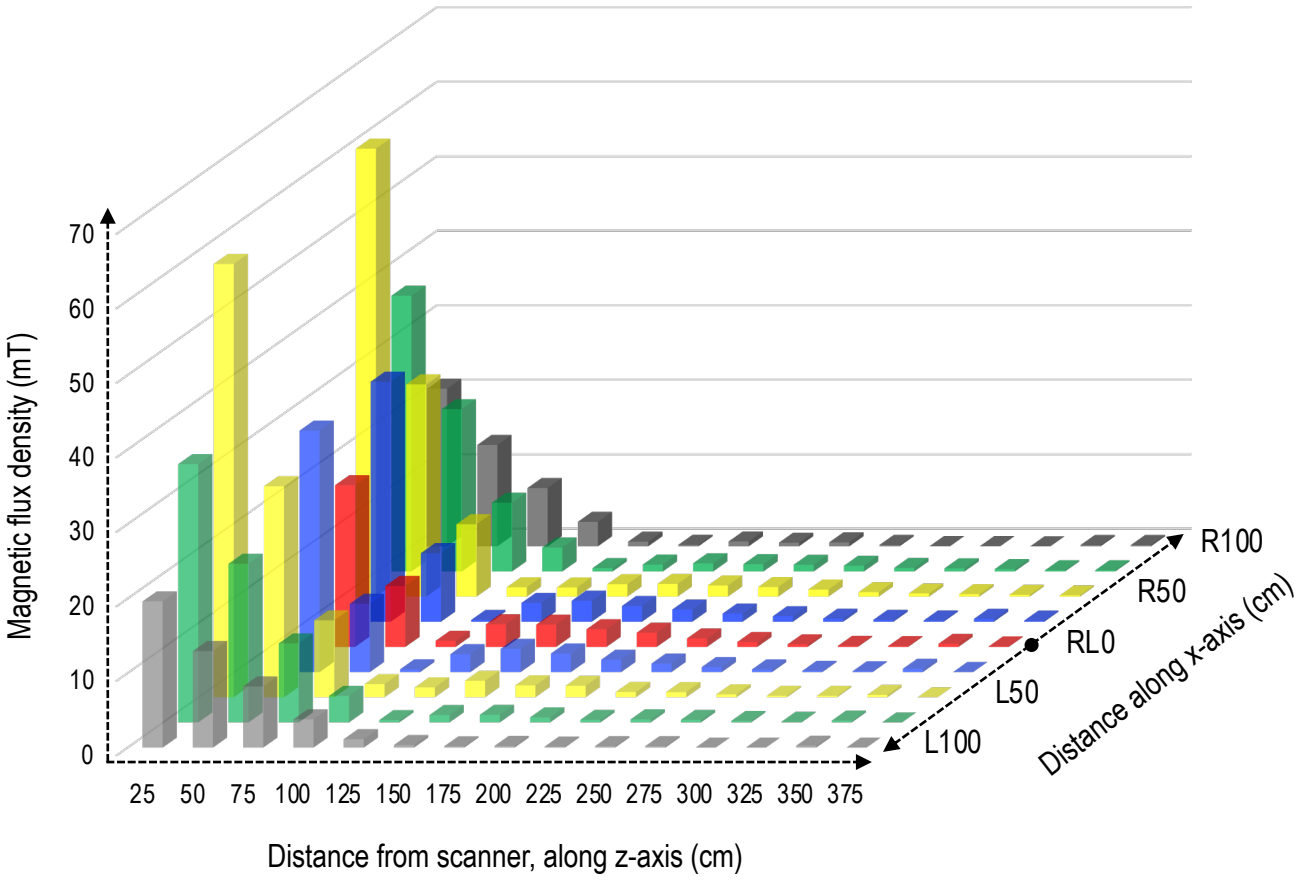


Figure 4. Magnetic flux density (mT) at y=-100 cm (ground level)

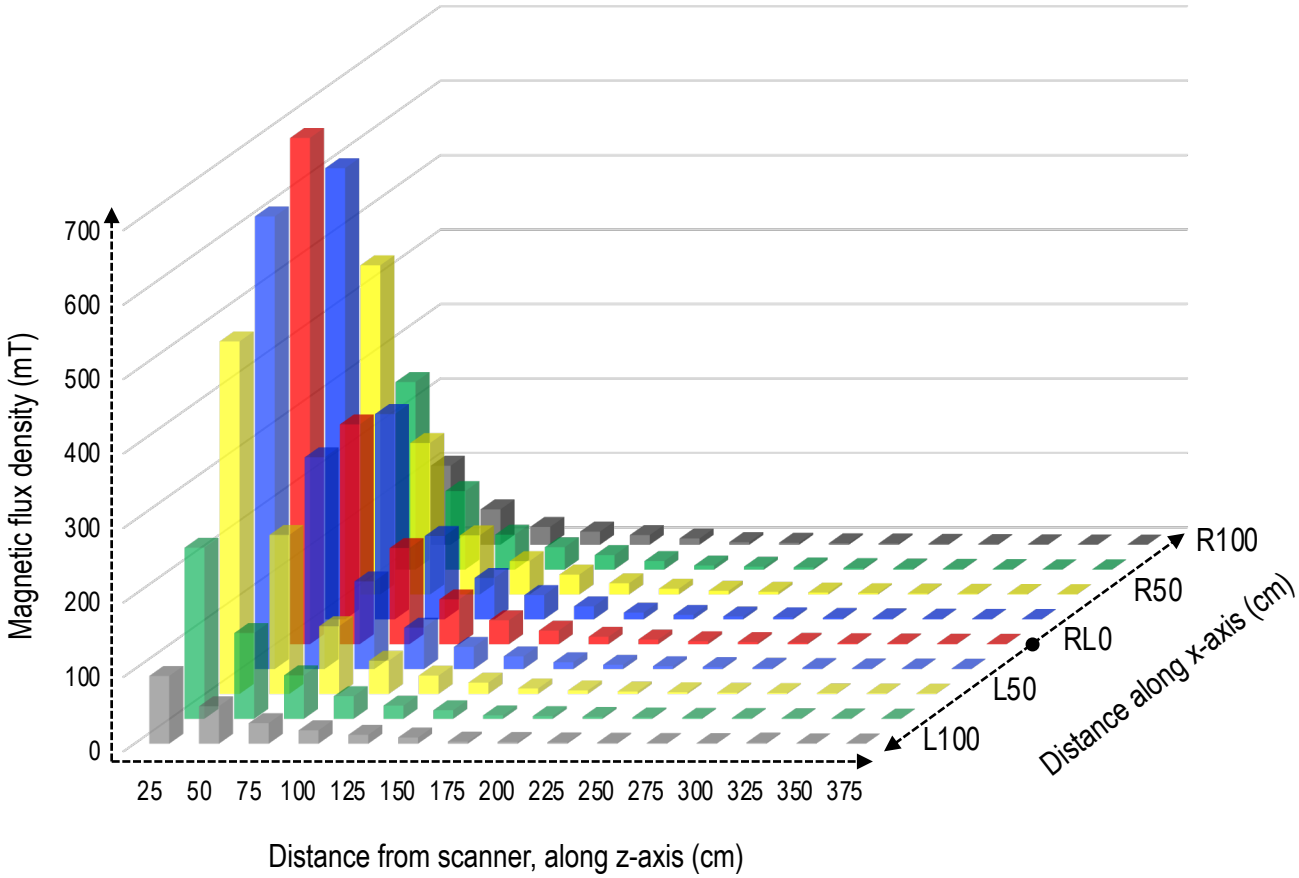


Figure 5. Magnetic flux density (mT) at y=0 cm (patient table level)

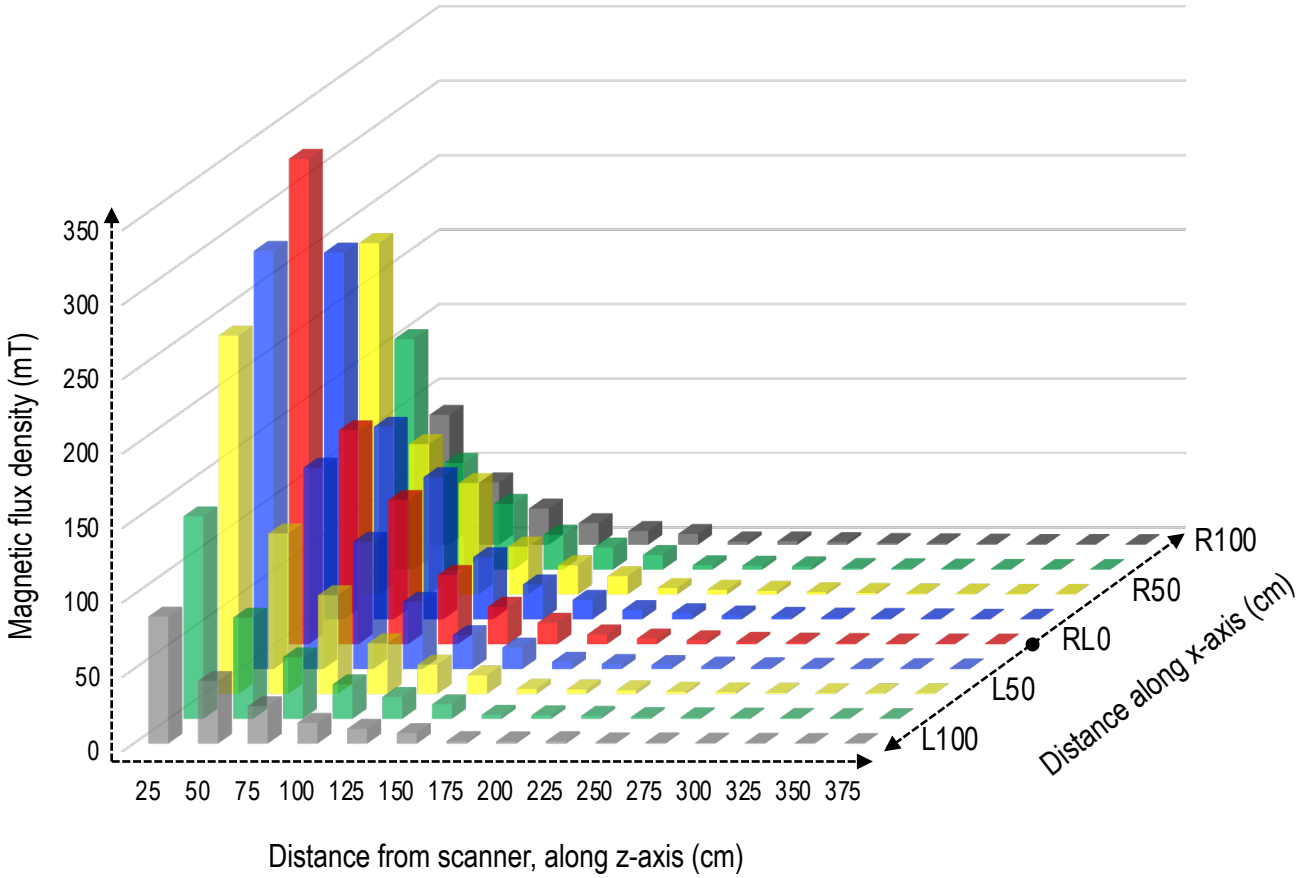


Figure 6. Magnetic flux density (mT) at y=50 cm (patient height level)

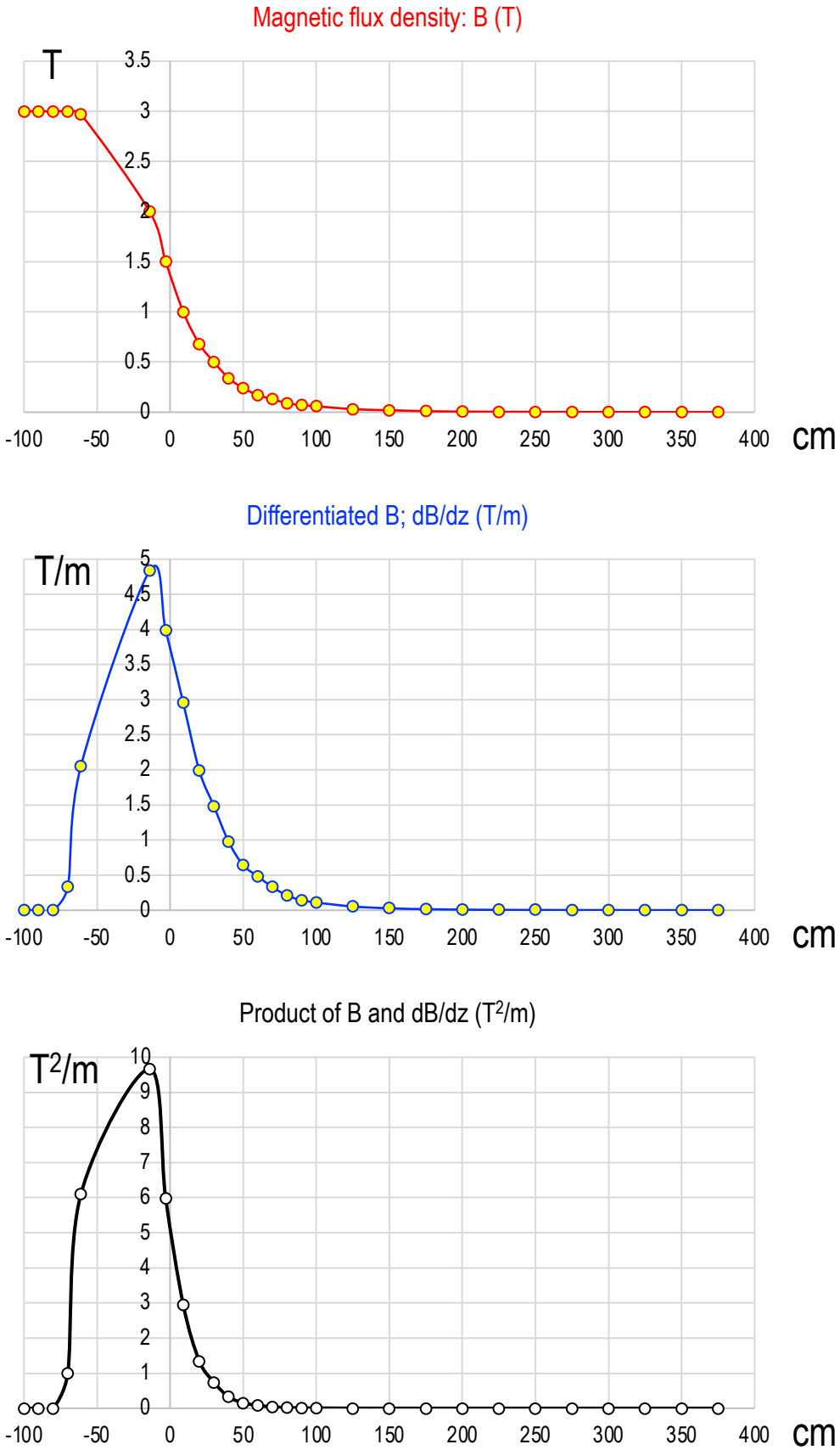


Figure 7. B, dB/dz, and their product

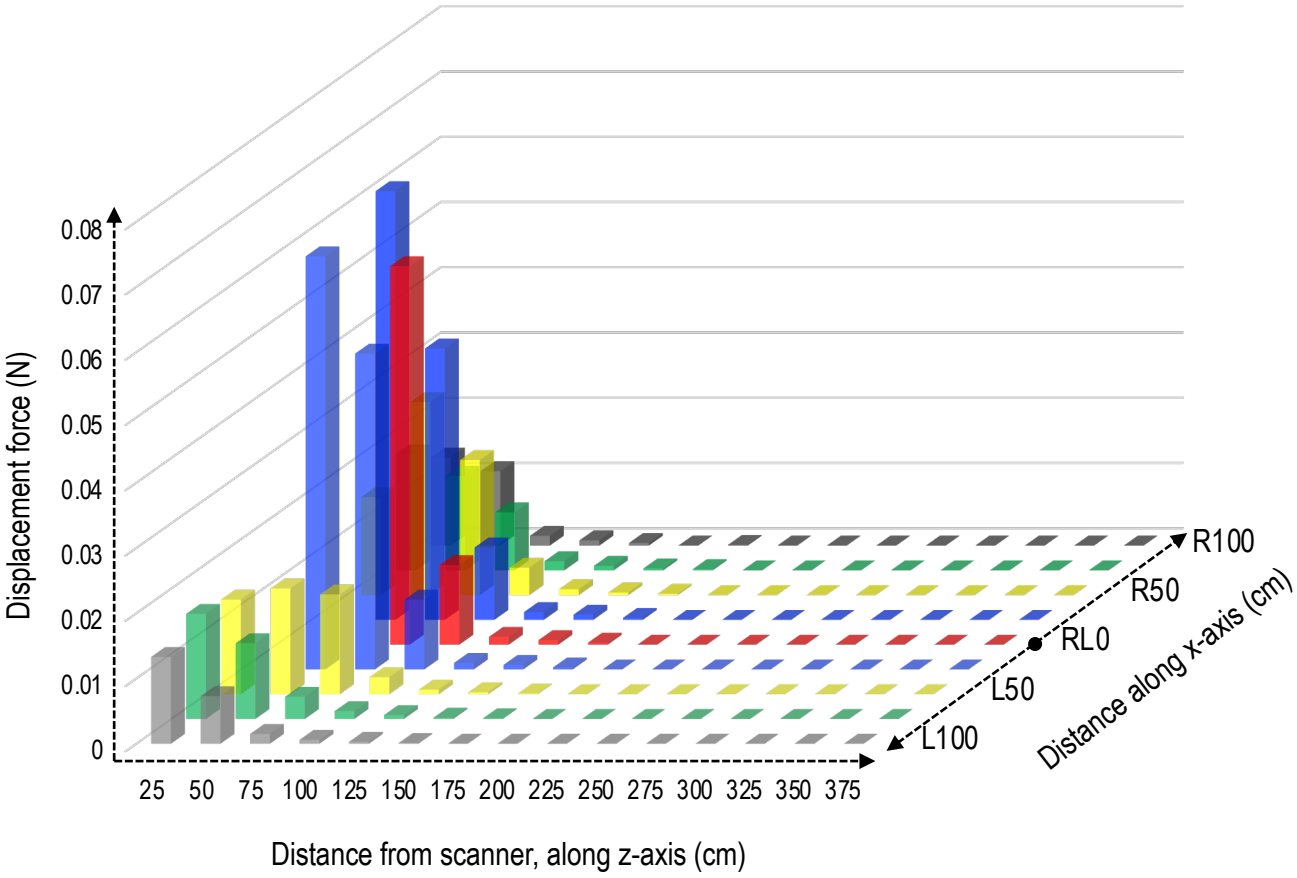


Figure 8. Displacement force (N) at y=-100 cm (ground level)

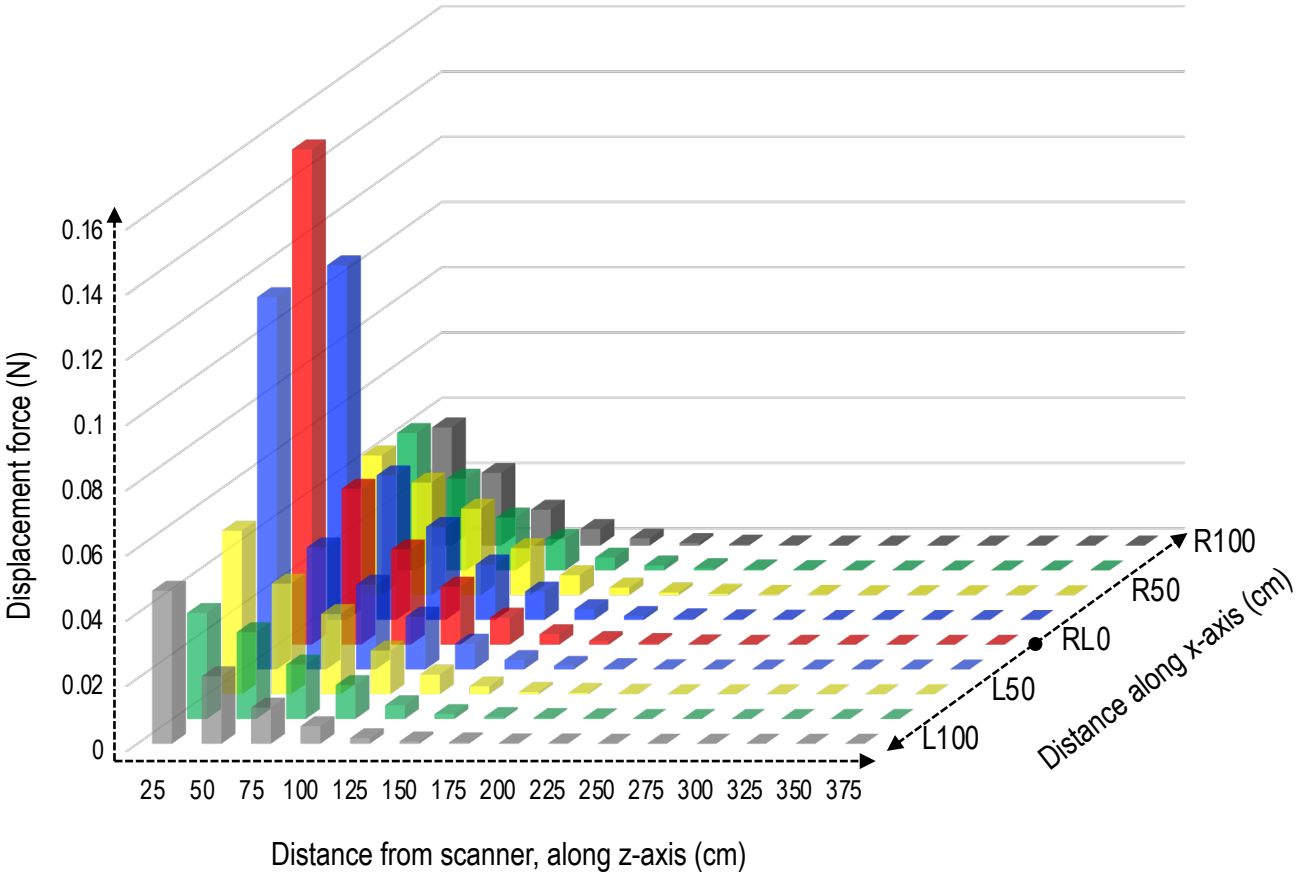


Figure 9. Displacement force (N) at y=0 cm (patient table level)

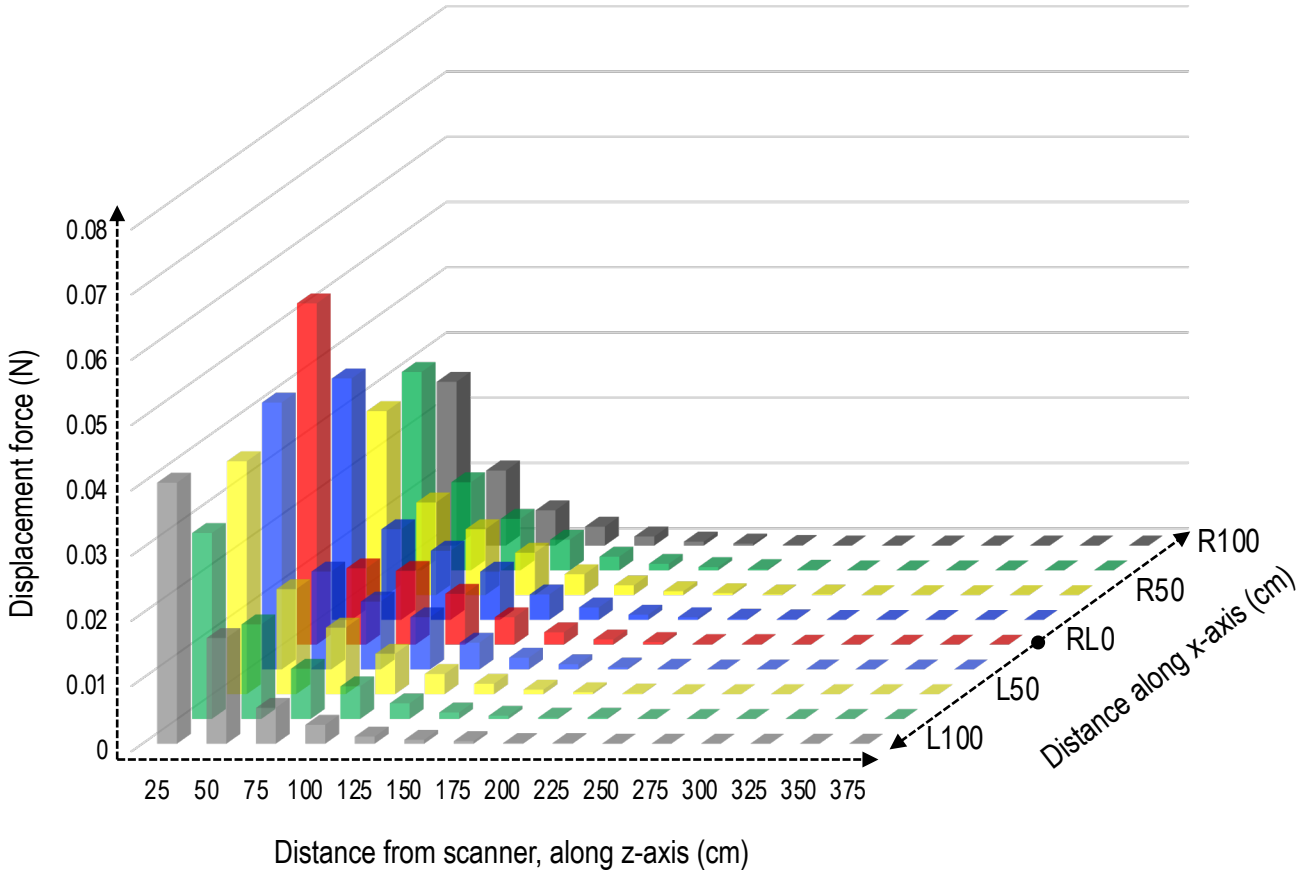


Figure 10. Displacement force (N) at y=50 cm (patient height level)

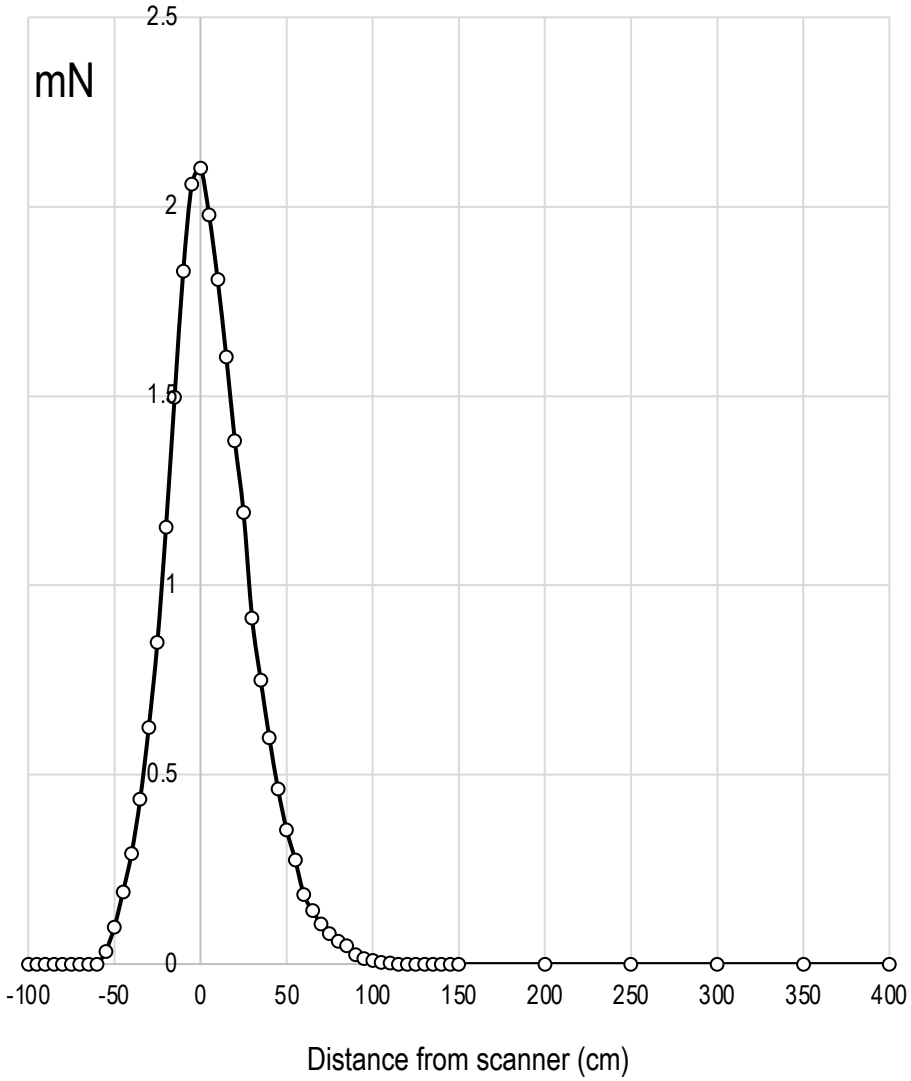


"0 cm" means the edge of the gantry.
"−100 cm" is the center of the gantry.

Figure 11. Displacement force along gantry center (mN)

Displacement force on Dental materials

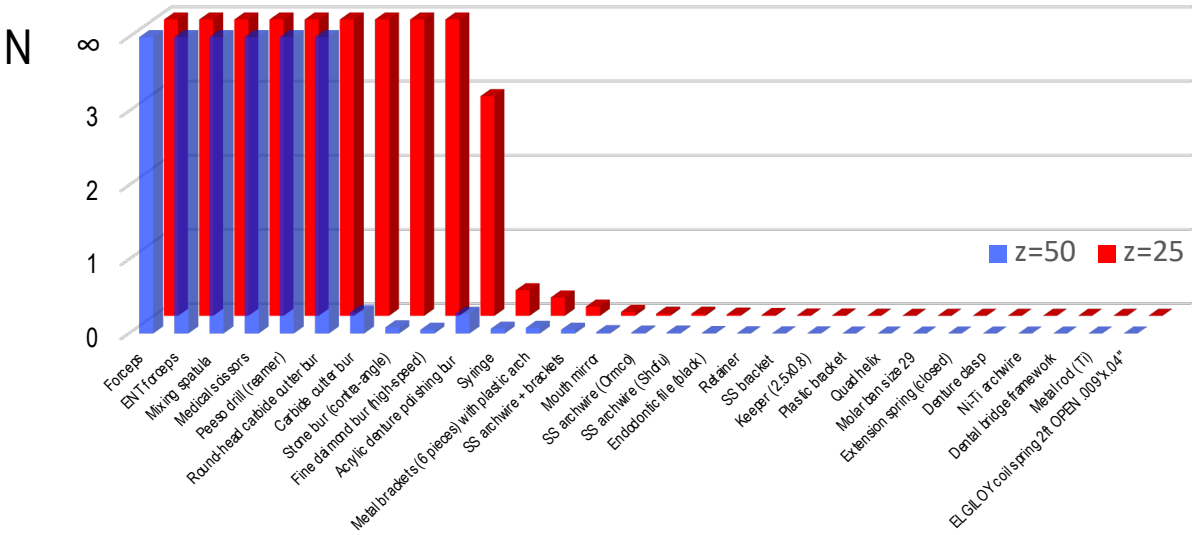


Displacement force on Household items

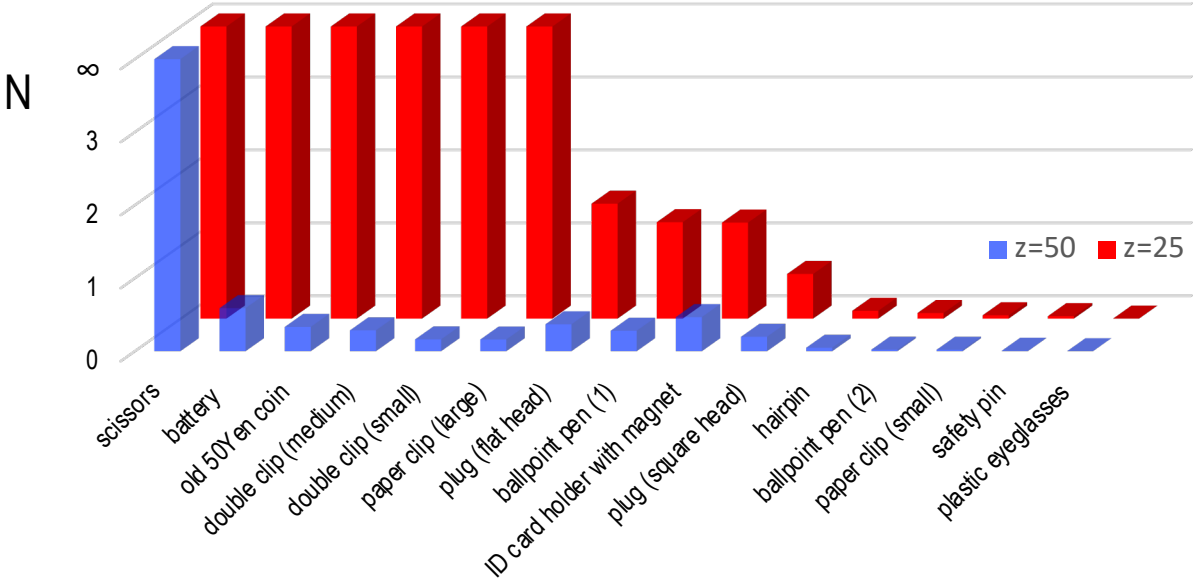


Note:

Tested materials that their bars reached ∞ were the materials that exhibited the deflection angle (θ) equal to or more than 90 degrees and their displacement forces were incalculable according to the equation $F_{disp} = W_{mat} \cdot \tan \theta$ (in Figure 2.)

Figure 12. Displacement force on materials (N) at z= 25 and 50 cm

Table 1 Tested materials for displacement force measuremenent

| Dental materials | | Chief component |
|---|---|---|
| D1 | Cotton pliers (forceps) | SS |
| D2 | ENT forceps | SS |
| D3 | Mixing spatula | SS |
| D4 | Medical scissors | SS |
| D5 | Peeso drill (reamer) | SS |
| D6 | Round-head carbide cutter bur | SS |
| D7 | Carbide cutter bur | SS |
| D8 | Stone bur (contra-angle) | SS |
| D9 | Fine daimond bur (high-speed) | SS |
| D10 | Acrylic denture polishing bur | SS |
| D11 | Endodontic file (black) | SS |
| D12 | ORTHOLINE Archwire .017x.025 (SHOFU) | SS |
| D13 | Preformed Achwires .017x.025 (Ormco) | SS |
| D14 | BENDALOY® Preformed Natural Arch .017x.025 (RMO) | Ni-Ti |
| D15 | Mini-Taurus® bracket (RMO) | SS |
| D16 | Plastic bracket | SS |
| D17 | Archwire and brackets (6 SS and 6 plastic brackets) with a plastic arch | SS |
| D18 | Brackets (6) with a plastic arch | SS |
| D19 | ELGILOY® coil spring 2ft OPEN .009"x.04" | Co-Cr-Ni-Mo |
| D20 | Extension spring (closed coil) .012x.030 / 12 mm (RMO) | Ni-Ti |
| D21 | Maxillary Quad Helix (Ricketts®) size 3 (RMO) | Co-Cr-Ni-Mo |
| D22 | Retainer | SS |
| D23 | TRUFORM universal molar ban (size 29) (RMO) | SS |
| D24 | PHYSIO MAGNET keeper 2.5x0.8 mm (MORITA) | Fe, Cr(30%) |
| D25 | Denture clasp | Co-Cr |
| D26 | Dental bridge framework | Au-Ag-Pd |
| D27 | Syringe | SS |
| D28 | Mouth mirror | SS |
| D29 | Rod-shaped metal (3x3x13mm) | Ti |
| Household items | | Chief component |
| H1 | Scissors | SS |
| H2 | Double clip (medium size) | SS |
| H3 | Double clip (small size) | SS |
| H4 | Paper clip (large) | SS |
| H5 | Paper clip (small) | SS |
| H6 | 50-Yen coin (previous version) | Cu-Ni |
| H7 | Battery (AAA size) | steel |
| H8 | Ballpoint pen (1) | unknown |
| H9 | Ballpoint pen (2) | unknown |
| H10 | Plastic eyeglasses | no metal component |
| H11 | Hairpin | steel |
| H12 | Safety pin | SS |
| H13 | Electrical plug (1) | unknown |
| H14 | Electrical plug (2) | unknown |
| H15 | ID card holder with magnet | Fe-Ni-Co (magnet) |

SS: stainless steel

Table 2 Tested materials for torque measuremenent

| Dental materials | | Chief component |
|---|---|---|
| D1 | Tru-Chrome® Preformed Natural Arches .017x.025 (RMO) | SS |
| D2 | Tru-Chrome® Preformed Natural Arches .016x.016 (RMO) | SS |
| D3 | ORTHOLINE Archwire .017x.025 (SHOFU) | SS |
| D4 | Permachrome Resilient, OrthoForm™ II, .017x.025 (3M™ Unitek™) | SS |
| D5 | Preformed Achwires .017x.025 (Ormco) | SS |
| D6 | FLI® Preformed Natural Arch .017x.025 (RMO) | SS |
| D7 | FLI® Preformed Natural Arch .016x.016 (RMO) | SS |
| D8 | GUMMETAL® White Arch Wire 0.406x0.406 mm (JM ortho) | Ti-Nb |
| D9 | ELGILOY® Blue Preformed natural arch .017x.025 (RMO) | Co-Cr-Ni-Mo |
| D10 | BENDALOY® Preformed Natural Arch .017x.025 (RMO) | Ni-Ti |
| D11 | Extension spring (closed coil) .012x.030 / 12 mm (RMO) | Ni-Ti |
| D12 | Maxillary Quad Helix (Ricketts®) size 3 (RMO) | Co-Cr-Ni-Mo |
| Household items | | Chief component |
| H1 | Hair pin | Fe |
| H2 | Paper clip | Fe |

SS: stainless steel

Table 3 Magnetic flux density (mT) at y=-100 cm (ground level)

| | x-cordinate (cm) | | | | | | | | |
|---|---|---|---|---|---|---|---|---|---|
| | -100<br>left 100 | -75<br>left 75 | -50<br>left 50 | -25<br>left 25 | 0<br>center | 25<br>right 25 | 50<br>right 50 | 75<br>right 75 | 100<br>right 100 |
| z-cordinate (cm) | | | | | | | | | |
| 25 | 19.6<br>(0.2) | 34.7<br>(0.2) | 58.2<br>(0.1) | NA | NA | NA | 60.1<br>(0.1) | 37.0<br>(0.1) | 21.2<br>(0.1) |
| 50 | 13.0<br>(0.3) | 21.3<br>(0.6) | 28.3<br>(0.1) | 32.4<br>(0.6) | 21.7<br>(4.9) | 32.2<br>(0.9) | 28.5<br>(0.4) | 21.8<br>(0.5) | 13.6<br>(0.5) |
| 75 | 8.2<br>(0.1) | 10.6<br>(0.3) | 10.3<br>(0.7) | 9.2<br>(0.6) | 8.2<br>(1.0) | 9.2<br>(0.4) | 9.7<br>(0.9) | 9.2<br>(0.7) | 7.8<br>(0.4) |
| 100 | 3.8<br>(0.2) | 3.6<br>(0.2) | 1.8<br>(0.6) | 0.4<br>(0.6) | 0.8<br>(0.3) | 0.3<br>(0.1) | 1.3<br>(0.4) | 3.2<br>(0.3) | 3.3<br>(0.4) |
| 125 | 1.1<br>(0.3) | 0.3<br>(0.3) | 1.3<br>(0.2) | 2.4<br>(0.1) | 3.1<br>(0.4) | 2.5<br>(0.2) | 1.2<br>(0.3) | 0.5<br>(0.3) | 0.6<br>(0.5) |
| 150 | 0.4<br>(0.1) | 1.0<br>(0.2) | 2.2<br>(0.0) | 3.1<br>(0.1) | 3.0<br>(0.2) | 2.8<br>(0.2) | 1.7<br>(0.3) | 0.9<br>(0.4) | 0.2<br>(0.2) |
| 175 | 0.2<br>(0.7) | 1.0<br>(1.4) | 1.6<br>(2.1) | 2.5<br>(2.9) | 2.4<br>(1.8) | 2.1<br>(1.9) | 1.7<br>(2.7) | 1.1<br>(2.2) | 0.7<br>(1.3) |
| 200 | 0.2<br>(1.2) | 0.7<br>(0.7) | 1.6<br>(1.4) | 1.7<br>(1.6) | 1.9<br>(1.8) | 1.7<br>(1.5) | 1.5<br>(1.9) | 1.0<br>(1.3) | 0.5<br>(0.9) |
| 225 | 0.2<br>(1.5) | 0.4<br>(1.3) | 0.7<br>(1.1) | 1.2<br>(1.0) | 1.2<br>(0.9) | 1.1<br>(1.2) | 1.3<br>(1.0) | 0.9<br>(0.5) | 0.5<br>(0.5) |
| 250 | 0.2<br>(0.2) | 0.4<br>(0.5) | 0.7<br>(0.8) | 0.7<br>(0.9) | 0.7<br>(0.9) | 0.8<br>(0.7) | 1.0<br>(0.8) | 0.8<br>(0.8) | 0.2<br>(0.5) |
| 275 | 0.2<br>(0.2) | 0.4<br>(0.1) | 0.4<br>(0.3) | 0.4<br>(0.4) | 0.4<br>(0.6) | 0.4<br>(0.5) | 0.6<br>(0.5) | 0.5<br>(0.2) | 0.0<br>(0.3) |
| 300 | 0.0<br>(0.4) | 0.2<br>(0.3) | 0.2<br>(0.3) | 0.2<br>(0.3) | 0.2<br>(0.4) | 0.3<br>(0.2) | 0.4<br>(0.4) | 0.4<br>(0.3) | 0.0<br>(0.5) |
| 325 | 0.0<br>(0.6) | 0.1<br>(0.5) | 0.2<br>(0.4) | 0.1<br>(0.4) | 0.1<br>(0.4) | 0.2<br>(0.3) | 0.3<br>(0.4) | 0.3<br>(0.5) | 0.0<br>(0.5) |
| 350 | 0.3<br>(0.6) | 0.3<br>(0.6) | 0.3<br>(0.5) | 0.5<br>(0.5) | 0.4<br>(0.4) | 0.4<br>(0.4) | 0.3<br>(0.5) | 0.2<br>(0.6) | 0.2<br>(0.5) |
| 375 | 0.0<br>(0.6) | 0.0<br>(0.6) | 0.0<br>(0.5) | 0.0<br>(0.5) | 0.1<br>(0.6) | 0.2<br>(0.5) | 0.2<br>(0.5) | 0.2<br>(0.6) | 0.2<br>(0.6) |

Values are average of 6-time measurements.
Values in parenthesis are standard deviation.

NA: Measurement was impossible due to Table Base

Table 4 Magnetic flux density (mT) at y=0 cm (patient table level)

| | x-cordinate (cm) | | | | | | | | |
|---|---|---|---|---|---|---|---|---|---|
| | -100<br>left 100 | -75<br>left 75 | -50<br>left 50 | -25<br>left 25 | 0<br>center | 25<br>right 25 | 50<br>right 50 | 75<br>right 75 | 100<br>right 100 |
| z-cordinate (cm) | | | | | | | | | |
| 25 | 91.0<br>(0.6) | 229.8<br>(4.3) | 473.5<br>(14.4) | 608.0<br>(4.9) | 680.0<br>(0.6) | 606.0<br>(4.2) | 442.2<br>(8.0) | 252.0<br>(6.2) | 106.2<br>(3.9) |
| 50 | 50.3<br>(2.8) | 115.3<br>(2.7) | 213.7<br>(3.6) | 284.5<br>(2.7) | 295.3<br>(4.0) | 275.8<br>(2.7) | 203.5<br>(9.2) | 105.5<br>(3.4) | 47.5<br>(1.5) |
| 75 | 27.7<br>(1.8) | 58.5<br>(0.8) | 91.0<br>(1.1) | 117.8<br>(1.3) | 129.2<br>(0.8) | 112.0<br>(1.1) | 79.5<br>(0.5) | 47.0<br>(0.6) | 24.0<br>(1.1) |
| 100 | 17.9<br>(0.3) | 30.5<br>(0.3) | 44.7<br>(0.4) | 55.7<br>(0.2) | 60.3<br>(0.7) | 55.7<br>(0.5) | 44.8<br>(0.4) | 30.2<br>(0.4) | 17.7<br>(0.5) |
| 125 | 11.9<br>(0.2) | 17.8<br>(0.2) | 24.7<br>(0.3) | 29.9<br>(0.2) | 32.2<br>(0.2) | 32.7<br>(0.5) | 26.8<br>(0.4) | 19.6<br>(0.3) | 13.0<br>(0.3) |
| 150 | 8.3<br>(0.1) | 11.6<br>(0.1) | 15.3<br>(0.2) | 17.1<br>(0.2) | 18.4<br>(0.3) | 17.5<br>(0.2) | 15.1<br>(0.0) | 11.6<br>(0.1) | 8.5<br>(0.2) |
| 175 | 2.8<br>(0.5) | 4.7<br>(0.5) | 7.4<br>(0.4) | 9.2<br>(0.5) | 10.0<br>(0.5) | 9.1<br>(0.4) | 7.8<br>(0.5) | 5.6<br>(0.7) | 3.5<br>(0.6) |
| 200 | 2.4<br>(0.3) | 3.7<br>(0.2) | 4.8<br>(0.2) | 5.9<br>(0.3) | 6.4<br>(0.3) | 6.0<br>(0.2) | 5.0<br>(0.1) | 4.0<br>(0.2) | 2.7<br>(0.5) |
| 225 | 1.8<br>(0.2) | 2.7<br>(0.2) | 3.4<br>(0.2) | 3.9<br>(0.2) | 4.1<br>(0.2) | 4.0<br>(0.2) | 3.6<br>(0.3) | 3.0<br>(0.4) | 2.1<br>(0.3) |
| 250 | 1.3<br>(0.2) | 1.9<br>(0.1) | 2.4<br>(0.1) | 2.8<br>(0.1) | 2.9<br>(0.1) | 2.8<br>(0.1) | 2.6<br>(0.3) | 2.1<br>(0.2) | 1.7<br>(0.3) |
| 275 | 1.0<br>(0.2) | 1.4<br>(0.2) | 1.7<br>(0.1) | 1.9<br>(0.0) | 2.0<br>(0.1) | 2.0<br>(0.2) | 1.8<br>(0.2) | 1.5<br>(0.2) | 1.2<br>(0.3) |
| 300 | 0.8<br>(0.1) | 1.1<br>(0.2) | 1.3<br>(0.2) | 1.5<br>(0.2) | 1.5<br>(0.2) | 1.4<br>(0.3) | 1.3<br>(0.2) | 1.2<br>(0.2) | 0.9<br>(0.2) |
| 325 | 1.5<br>(2.4) | 0.9<br>(0.2) | 0.9<br>(0.2) | 1.0<br>(0.0) | 1.1<br>(0.2) | 1.1<br>(0.2) | 1.0<br>0.0 | 0.8<br>(0.2) | 0.6<br>(0.3) |
| 350 | 0.4<br>(0.1) | 0.6<br>(0.2) | 0.7<br>(0.2) | 0.8<br>(0.2) | 0.8<br>(0.2) | 0.8<br>(0.2) | 0.7<br>(0.0) | 0.5<br>(0.2) | 0.4<br>(0.2) |
| 375 | 0.3<br>(0.1) | 0.4<br>(0.1) | 0.6<br>(0.2) | 0.7<br>(0.2) | 0.7<br>(0.1) | 0.6<br>(0.2) | 0.5<br>(0.2) | 0.5<br>(0.1) | 0.3<br>(0.1) |

Values are average of 6-time measurements.
Values in parenthesis are standard deviation.

Table 5 Magnetic flux density (mT) at y=50 cm (patient height level)

| | x-cordinate (cm) | | | | | | | | |
|---|---|---|---|---|---|---|---|---|---|
| | -100<br>left 100 | -75<br>left 75 | -50<br>left 50 | -25<br>left 25 | 0<br>center | 25<br>right 25 | 50<br>right 50 | 75<br>right 75 | 100<br>right 100 |
| z-cordinate (cm) | | | | | | | | | |
| 25 | 85.3<br>(3.1) | 136.0<br>(3.8) | 240.7<br>(3.5) | 280.8<br>(5.3) | 326.0<br>(13.0) | 246.3<br>(4.4) | 236.0<br>(6.2) | 154.8<br>(3.6) | 87.2<br>(3.3) |
| 50 | 42.2<br>(1.3) | 68.0<br>(4.0) | 107.8<br>(3.2) | 135.3<br>(2.4) | 143.7<br>(3.3) | 129.3<br>(1.0) | 101.0<br>(1.5) | 71.7<br>(3.3) | 41.8<br>(1.7) |
| 75 | 25.2<br>(0.4) | 41.3<br>(1.4) | 66.3<br>(1.2) | 85.5<br>(2.2) | 96.8<br>(2.5) | 95.5<br>(6.1) | 74.8<br>(2.2) | 44.2<br>(2.7) | 24.3<br>(2.7) |
| 100 | 14.0<br>(1.4) | 23.2<br>(1.7) | 34.0<br>(1.8) | 45.2<br>(0.8) | 46.5<br>(1.8) | 41.8<br>(1.0) | 32.2<br>(1.2) | 23.5<br>(1.4) | 14.5<br>(1.2) |
| 125 | 10.0<br>0.0 | 14.7<br>(0.5) | 19.7<br>(0.5) | 22.8<br>(0.4) | 25.2<br>(0.8) | 23.5<br>(0.8) | 19.7<br>(0.5) | 14.8<br>(0.4) | 9.3<br>(0.8) |
| 150 | 7.2<br>(0.7) | 9.8<br>(1.4) | 12.5<br>(2.1) | 14.5<br>(2.9) | 14.4<br>(1.8) | 13.1<br>(1.9) | 12.3<br>(2.7) | 9.9<br>(2.2) | 7.3<br>(1.3) |
| 175 | 1.8<br>(0.7) | 2.7<br>(1.4) | 3.5<br>(2.1) | 4.9<br>(2.9) | 6.6<br>(1.8) | 6.3<br>(1.9) | 4.3<br>(2.7) | 2.9<br>(2.2) | 2.2<br>(1.3) |
| 200 | 1.6<br>(1.2) | 2.4<br>(0.7) | 3.0<br>(1.4) | 3.5<br>(1.6) | 3.8<br>(1.8) | 4.1<br>(1.5) | 3.2<br>(1.9) | 2.7<br>(1.3) | 2.3<br>(0.9) |
| 225 | 1.7<br>(1.5) | 2.0<br>(1.3) | 2.5<br>(1.1) | 2.8<br>(1.0) | 2.7<br>(0.9) | 2.6<br>(1.2) | 2.4<br>(1.0) | 2.2<br>(0.5) | 1.8<br>(0.5) |
| 250 | 0.9<br>(0.2) | 1.2<br>(0.5) | 1.5<br>(0.8) | 1.7<br>(0.9) | 1.7<br>(0.9) | 1.7<br>(0.7) | 1.5<br>(0.8) | 1.1<br>(0.8) | 1.2<br>(0.5) |
| 275 | 0.9<br>(0.2) | 1.1<br>(0.1) | 1.2<br>(0.3) | 1.3<br>(0.4) | 1.1<br>(0.6) | 1.2<br>(0.5) | 1.1<br>(0.5) | 0.9<br>(0.2) | 1.0<br>(0.3) |
| 300 | 0.6<br>(0.4) | 0.8<br>(0.3) | 0.8<br>(0.3) | 0.9<br>(0.3) | 0.8<br>(0.4) | 0.9<br>(0.2) | 0.7<br>(0.4) | 0.7<br>(0.3) | 0.7<br>(0.5) |
| 325 | 0.6<br>(0.6) | 0.6<br>(0.5) | 0.6<br>(0.4) | 0.7<br>(0.4) | 0.5<br>(0.4) | 0.7<br>(0.3) | 0.6<br>(0.4) | 0.5<br>(0.5) | 0.5<br>(0.5) |
| 350 | 0.5<br>(0.6) | 0.6<br>(0.6) | 0.5<br>(0.5) | 0.7<br>(0.5) | 0.5<br>(0.4) | 0.4<br>(0.4) | 0.4<br>(0.5) | 0.4<br>(0.6) | 0.5<br>(0.5) |
| 375 | 0.4<br>(0.6) | 0.5<br>(0.6) | 0.5<br>(0.5) | 0.5<br>(0.5) | 0.5<br>(0.6) | 0.4<br>(0.5) | 0.4<br>(0.5) | 0.4<br>(0.6) | 0.5<br>(0.6) |

Values are average of 6-time measurements.
Values in parenthesis are standard deviation.

Table 6 Magnetic flux density along gantry centerline, and dB/dz, and their product

| | MFD (T) | dB／dz | product of MFD and dB／dz |
|---|---|---|---|
| z-cordinate (cm) | | | |
| -100 | 3.0000 | 0.0000 | 0.0000 |
| -90 | 3.0000 | 0.0000 | 0.0000 |
| -80 | 3.0000 | 0.0000 | 0.0000 |
| -70 | 3.0000 | 0.3330 | 1.0000 |
| -61 | 2.9700 | 2.0540 | 6.1010 |
| -14 | 2.0000 | 4.8360 | 9.6712 |
| -3 | 1.5000 | 3.9870 | 5.9809 |
| 9 | 1.0000 | 2.9540 | 2.9541 |
| 20 | 0.6800 | 1.9890 | 1.3484 |
| 30 | 0.5000 | 1.4810 | 0.7406 |
| 40 | 0.3400 | 0.9780 | 0.3290 |
| 50 | 0.2400 | 0.6430 | 0.1534 |
| 60 | 0.1700 | 0.4830 | 0.0842 |
| 70 | 0.1300 | 0.3300 | 0.0415 |
| 80 | 0.0900 | 0.2100 | 0.0195 |
| 90 | 0.0700 | 0.1420 | 0.0102 |
| 100 | 0.0600 | 0.1100 | 0.0063 |
| 125 | 0.0300 | 0.0530 | 0.0016 |
| 150 | 0.0200 | 0.0280 | 0.0005 |
| 175 | 0.0100 | 0.0150 | 0.0001 |
| 200 | 0.0060 | 0.0090 | 0.0001 |
| 225 | 0.0040 | 0.0050 | 0.0000 |
| 250 | 0.0030 | 0.0040 | 0.0000 |
| 275 | 0.0020 | 0.0020 | 0.0000 |
| 300 | 0.0015 | 0.0020 | 0.0000 |
| 325 | 0.0010 | 0.0010 | 0.0000 |
| 350 | 0.0008 | 0.0010 | 0.0000 |
| 375 | 0.0007 | 0.0000 | 0.0000 |

Values are average of 6-time measurements.

Table 7 Displacement force (mN) at y=-100 cm (ground level)

| | x-cordinate (cm) | | | | | | | | |
|---|---|---|---|---|---|---|---|---|---|
| | -100<br>left 100 | -75<br>left 75 | -50<br>left 50 | -25<br>left 25 | 0<br>center | 25<br>right 25 | 50<br>right 50 | 75<br>right 75 | 100<br>right 100 |
| z-cordinate (cm) | | | | | | | | | |
| 25 | 13.3<br>(0.0) | 16.1<br>(0.0) | 14.5<br>(0.0) | NA | NA | NA | 15.0<br>(0.0) | 17.8<br>(0.0) | 13.5<br>(0.0) |
| 50 | 7.3<br>(0.0) | 11.6<br>(0.0) | 16.2<br>(0.0) | 63.3<br>(0.0) | NA | 65.7<br>(0.0) | 29.6<br>(0.0) | 14.5<br>(0.0) | 11.4<br>(0.0) |
| 75 | 1.5<br>(0.0) | 3.4<br>(0.0) | 15.3<br>(0.0) | 48.4<br>(0.0) | 58.0<br>(0.0) | 41.6<br>(0.0) | 20.7<br>(0.0) | 8.9<br>(0.0) | 1.5<br>(0.0) |
| 100 | 0.6<br>(0.0) | 1.2<br>(0.0) | 2.6<br>(0.0) | 10.7<br>(0.0) | 12.2<br>(0.0) | 11.1<br>(0.0) | 4.2<br>(0.0) | 1.4<br>(0.0) | 0.8<br>(0.0) |
| 125 | 0.3<br>(0.0) | 0.6<br>(0.0) | 0.7<br>(0.0) | 1.0<br>(0.0) | 1.2<br>(0.0) | 1.2<br>(0.0) | 0.9<br>(0.0) | 0.7<br>(0.0) | 0.4<br>(0.0) |
| 150 | 0.1<br>(0.0) | 0.2<br>(0.0) | 0.3<br>(0.0) | 0.7<br>(0.0) | 0.7<br>(0.0) | 0.8<br>(0.0) | 0.4<br>(0.0) | 0.3<br>(0.0) | 0.0<br>(0.0) |
| 175 | 0.0<br>(0.0) | 0.1<br>(0.0) | 0.1<br>(0.0) | 0.3<br>(0.0) | 0.3<br>(0.0) | 0.3<br>(0.0) | 0.2<br>(0.0) | 0.2<br>(0.0) | 0.1<br>(0.0) |
| 200 | 0.0<br>(0.0) | 0.0<br>(0.0) | 0.0<br>(0.0) | 0.0<br>(0.0) | 0.0<br>(0.0) | 0.0<br>(0.0) | 0.0<br>(0.0) | 0.0<br>(0.0) | 0.0<br>(0.0) |
| 225 | 0.0<br>(0.0) | 0.0<br>(0.0) | 0.0<br>(0.0) | 0.0<br>(0.0) | 0.0<br>(0.0) | 0.0<br>(0.0) | 0.0<br>(0.0) | 0.0<br>(0.0) | 0.0<br>(0.0) |
| 250 | 0.0<br>(0.0) | 0.0<br>(0.0) | 0.0<br>(0.0) | 0.0<br>(0.0) | 0.0<br>(0.0) | 0.0<br>(0.0) | 0.0<br>(0.0) | 0.0<br>(0.0) | 0.0<br>(0.0) |
| 275 | 0.0<br>(0.0) | 0.0<br>(0.0) | 0.0<br>(0.0) | 0.0<br>(0.0) | 0.0<br>(0.0) | 0.0<br>(0.0) | 0.0<br>(0.0) | 0.0<br>(0.0) | 0.0<br>(0.0) |
| 300 | 0.0<br>(0.0) | 0.0<br>(0.0) | 0.0<br>(0.0) | 0.0<br>(0.0) | 0.0<br>(0.0) | 0.0<br>(0.0) | 0.0<br>(0.0) | 0.0<br>(0.0) | 0.0<br>(0.0) |
| 325 | 0.0<br>(0.0) | 0.0<br>(0.0) | 0.0<br>(0.0) | 0.0<br>(0.0) | 0.0<br>(0.0) | 0.0<br>(0.0) | 0.0<br>(0.0) | 0.0<br>(0.0) | 0.0<br>(0.0) |
| 350 | 0.0<br>(0.0) | 0.0<br>(0.0) | 0.0<br>(0.0) | 0.0<br>(0.0) | 0.0<br>(0.0) | 0.0<br>(0.0) | 0.0<br>(0.0) | 0.0<br>(0.0) | 0.0<br>(0.0) |
| 375 | 0.0<br>(0.0) | 0.0<br>(0.0) | 0.0<br>(0.0) | 0.0<br>(0.0) | 0.0<br>(0.0) | 0.0<br>(0.0) | 0.0<br>(0.0) | 0.0<br>(0.0) | 0.0<br>(0.0) |

Numbers are calculated values from the average of 6-time measurements of deflection angle.
Values in parenthesis are standard deviation.

NA: Measurement was impossible due to Table Base

Table 8 Displacement force (mN) at y=0 cm (patient table level)

| | x-cordinate (cm) | | | | | | | | |
|---|---|---|---|---|---|---|---|---|---|
| | -100<br>left 100 | -75<br>left 75 | -50<br>left 50 | -25<br>left 25 | 0<br>center | 25<br>right 25 | 50<br>right 50 | 75<br>right 75 | 100<br>right 100 |
| z-cordinate (cm) | | | | | | | | | |
| 25 | 46.9<br>(0.0) | 32.5<br>(0.0) | 50.1<br>(0.0) | 114.1<br>(0.0) | 151.8<br>(0.0) | 108.7<br>(0.0) | 42.8<br>(0.1) | 42.1<br>(0.0) | 36.2<br>(0.0) |
| 50 | 20.7<br>(0.0) | 26.6<br>(0.0) | 33.9<br>(0.0) | 37.4<br>(0.0) | 47.8<br>(0.0) | 44.3<br>(0.0) | 34.5<br>(0.0) | 28.1<br>(0.0) | 22.3<br>(0.0) |
| 75 | 11.1<br>(0.0) | 16.7<br>(0.1) | 24.6<br>(0.0) | 26.0<br>(0.1) | 29.2<br>(0.0) | 28.5<br>(0.0) | 26.5<br>(0.0) | 16.2<br>(0.1) | 11.0<br>(0.0) |
| 100 | 5.4<br>(0.0) | 10.4<br>(0.0) | 13.4<br>(0.0) | 16.2<br>(0.0) | 17.8<br>(0.1) | 17.0<br>(0.0) | 14.4<br>(0.0) | 9.6<br>(0.0) | 5.1<br>(0.0) |
| 125 | 1.7<br>(0.0) | 4.2<br>(0.1) | 6.0<br>(0.1) | 7.9<br>(0.0) | 8.3<br>(0.2) | 8.7<br>(0.0) | 6.1<br>(0.0) | 3.9<br>(0.2) | 2.2<br>(0.0) |
| 150 | 0.7<br>(0.0) | 1.5<br>(0.0) | 2.4<br>(0.0) | 2.9<br>(0.1) | 3.2<br>(0.1) | 3.3<br>(0.0) | 2.3<br>(0.0) | 1.5<br>(0.0) | 0.8<br>(0.0) |
| 175 | 0.4<br>(0.0) | 0.6<br>(0.0) | 0.7<br>(0.0) | 1.1<br>(0.1) | 1.1<br>(0.1) | 1.2<br>(0.0) | 0.8<br>(0.0) | 0.7<br>(0.0) | 0.3<br>(0.0) |
| 200 | 0.1<br>(0.0) | 0.3<br>(0.0) | 0.4<br>(0.0) | 0.4<br>(0.1) | 0.5<br>(0.1) | 0.5<br>(0.0) | 0.4<br>(0.0) | 0.3<br>(0.0) | 0.1<br>(0.0) |
| 225 | 0.1<br>(0.0) | 0.2<br>(0.0) | 0.1<br>(0.0) | 0.1<br>(0.0) | 0.1<br>(0.0) | 0.2<br>(0.0) | 0.1<br>(0.0) | 0.1<br>(0.0) | 0.0<br>(0.0) |
| 250 | 0.0<br>(0.0) | 0.0<br>(0.0) | 0.0<br>(0.0) | 0.0<br>(0.0) | 0.0<br>(0.0) | 0.1<br>(0.0) | 0.1<br>(0.0) | 0.0<br>(0.0) | 0.0<br>(0.0) |
| 275 | 0.0<br>(0.0) | 0.0<br>(0.0) | 0.0<br>(0.0) | 0.0<br>(0.0) | 0.0<br>(0.0) | 0.0<br>(0.0) | 0.0<br>(0.0) | 0.0<br>(0.0) | 0.0<br>(0.0) |
| 300 | 0.0<br>(0.0) | 0.0<br>(0.0) | 0.0<br>(0.0) | 0.0<br>(0.0) | 0.0<br>(0.0) | 0.0<br>(0.0) | 0.0<br>(0.0) | 0.0<br>(0.0) | 0.0<br>(0.0) |
| 325 | 0.0<br>(0.0) | 0.0<br>(0.0) | 0.0<br>(0.0) | 0.0<br>(0.0) | 0.0<br>(0.0) | 0.0<br>(0.0) | 0.0<br>(0.0) | 0.0<br>(0.0) | 0.0<br>(0.0) |
| 350 | 0.0<br>(0.0) | 0.0<br>(0.0) | 0.0<br>(0.0) | 0.0<br>(0.0) | 0.0<br>(0.0) | 0.0<br>(0.0) | 0.0<br>(0.0) | 0.0<br>(0.0) | 0.0<br>(0.0) |
| 375 | 0.0<br>(0.0) | 0.0<br>(0.0) | 0.0<br>(0.0) | 0.0<br>(0.0) | 0.0<br>(0.0) | 0.0<br>(0.0) | 0.0<br>(0.0) | 0.0<br>(0.0) | 0.0<br>(0.0) |

Numbers are calculated values from the average of 6-time measurements of deflection angle.
Values in parenthesis are standard deviation.

Table 9 Displacement force (mN) at y=50 cm (patient height level)

| | x-cordinate (cm) | | | | | | | | |
|---|---|---|---|---|---|---|---|---|---|
| | -100<br>left 100 | -75<br>left 75 | -50<br>left 50 | -25<br>left 25 | 0<br>center | 25<br>right 25 | 50<br>right 50 | 75<br>right 75 | 100<br>right 100 |
| z-cordinate (cm) | | | | | | | | | |
| 25 | 40.0<br>(0.0) | 28.5<br>(0.0) | 35.7<br>(0.0) | 40.9<br>(0.0) | 52.3<br>(0.0) | 37.0<br>(0.0) | 28.2<br>(0.0) | 30.4<br>(0.0) | 25.1<br>(0.0) |
| 50 | 16.2<br>(0.0) | 14.5<br>(0.0) | 16.1<br>(0.3) | 15.0<br>(0.0) | 11.7<br>(0.0) | 13.9<br>(0.0) | 14.2<br>(0.0) | 13.5<br>(0.0) | 11.5<br>(0.1) |
| 75 | 5.5<br>(0.0) | 7.7<br>(0.0) | 10.2<br>(0.0) | 10.4<br>(0.0) | 11.3<br>(0.0) | 10.6<br>(0.0) | 10.1<br>(0.0) | 7.9<br>(0.0) | 5.4<br>(0.0) |
| 100 | 2.9<br>(0.0) | 5.0<br>(0.1) | 6.2<br>(0.0) | 8.0<br>(0.2) | 7.8<br>(0.0) | 7.4<br>(0.0) | 6.5<br>(0.0) | 4.7<br>(0.0) | 2.9<br>(0.0) |
| 125 | 1.1<br>(0.0) | 2.4<br>(0.1) | 3.1<br>(0.0) | 4.1<br>(0.0) | 4.2<br>(0.0) | 3.9<br>(0.0) | 3.2<br>(0.0) | 2.1<br>(0.1) | 1.4<br>(0.0) |
| 150 | 0.6<br>(0.0) | 1.0<br>(0.0) | 1.6<br>(0.0) | 1.8<br>(0.0) | 1.9<br>(0.0) | 1.9<br>(0.0) | 1.5<br>(0.0) | 1.0<br>(0.0) | 0.6<br>(0.0) |
| 175 | 0.4<br>(0.0) | 0.5<br>(0.0) | 0.7<br>(0.0) | 0.8<br>(0.0) | 0.8<br>(0.0) | 0.8<br>(0.0) | 0.6<br>(0.0) | 0.5<br>(0.0) | 0.3<br>(0.0) |
| 200 | 0.1<br>(0.0) | 0.2<br>(0.0) | 0.3<br>(0.0) | 0.3<br>(0.0) | 0.4<br>(0.0) | 0.4<br>(0.0) | 0.3<br>(0.0) | 0.2<br>(0.0) | 0.1<br>(0.0) |
| 225 | 0.1<br>(0.0) | 0.2<br>(0.0) | 0.1<br>(0.0) | 0.1<br>(0.0) | 0.1<br>(0.0) | 0.2<br>(0.0) | 0.1<br>(0.0) | 0.1<br>(0.0) | 0.0<br>(0.0) |
| 250 | 0.0<br>(0.0) | 0.0<br>(0.0) | 0.0<br>(0.0) | 0.0<br>(0.0) | 0.1<br>(0.0) | 0.1<br>(0.0) | 0.1<br>(0.0) | 0.0<br>(0.0) | 0.0<br>(0.0) |
| 275 | 0.0<br>(0.0) | 0.0<br>(0.0) | 0.0<br>(0.0) | 0.0<br>(0.0) | 0.0<br>(0.0) | 0.0<br>(0.0) | 0.0<br>(0.0) | 0.0<br>(0.0) | 0.0<br>(0.0) |
| 300 | 0.0<br>(0.0) | 0.0<br>(0.0) | 0.0<br>(0.0) | 0.0<br>(0.0) | 0.0<br>(0.0) | 0.0<br>(0.0) | 0.0<br>(0.0) | 0.0<br>(0.0) | 0.0<br>(0.0) |
| 325 | 0.0<br>(0.0) | 0.0<br>(0.0) | 0.0<br>(0.0) | 0.0<br>(0.0) | 0.0<br>(0.0) | 0.0<br>(0.0) | 0.0<br>(0.0) | 0.0<br>(0.0) | 0.0<br>(0.0) |
| 350 | 0.0<br>(0.0) | 0.0<br>(0.0) | 0.0<br>(0.0) | 0.0<br>(0.0) | 0.0<br>(0.0) | 0.0<br>(0.0) | 0.0<br>(0.0) | 0.0<br>(0.0) | 0.0<br>(0.0) |
| 375 | 0.0<br>(0.0) | 0.0<br>(0.0) | 0.0<br>(0.0) | 0.0<br>(0.0) | 0.0<br>(0.0) | 0.0<br>(0.0) | 0.0<br>(0.0) | 0.0<br>(0.0) | 0.0<br>(0.0) |

Numbers are calculated values from the average of 6-time measurements of deflection angle.
Values in parenthesis are standard deviation.

Table 10 Diflection angle (degree) and Displacement force (mN) along gantry centerline

| z-cordinate (cm) | angle (degree) | displacement force (mN) | z-cordinate (cm) | angle (degree) | displacement force (mN) |
|---|---|---|---|---|---|
| -150 | 14.50 | 0.2790 | -15 | 54.23 | 1.4970 |
| -145 | 8.60 | 0.1630 | -10 | 59.48 | 1.8290 |
| -140 | 4.00 | 0.0750 | -5 | 62.37 | 2.0590 |
| -135 | 2.50 | 0.0470 | 0 | 62.85 | 2.1020 |
| -130 | 0.50 | 0.0090 | 5 | 61.42 | 1.9790 |
| -125 | 0.50 | 0.0090 | 10 | 59.18 | 1.8070 |
| -120 | 0.00 | 0.0000 | 15 | 56.10 | 1.6040 |
| -115 | 0.00 | 0.0000 | 20 | 52.03 | 1.3810 |
| -110 | 0.00 | 0.0000 | 25 | 47.90 | 1.1930 |
| -105 | 0.00 | 0.0000 | 30 | 40.25 | 0.9130 |
| -100 | 0.00 | 0.0000 | 35 | 34.83 | 0.7500 |
| -95 | 0.00 | 0.0000 | 40 | 29.02 | 0.5980 |
| -90 | 0.00 | 0.0000 | 45 | 23.25 | 0.4630 |
| -85 | 0.00 | 0.0000 | 50 | 18.25 | 0.3550 |
| -80 | 0.00 | 0.0000 | 55 | 14.32 | 0.2750 |
| -75 | 0.00 | 0.0000 | 60 | 9.68 | 0.1840 |
| -70 | 0.00 | 0.0000 | 65 | 7.45 | 0.1410 |
| -65 | 0.00 | 0.0000 | 70 | 5.63 | 0.1060 |
| -60 | 0.00 | 0.0000 | 75 | 4.30 | 0.0810 |
| -55 | 1.80 | 0.0340 | 80 | 3.25 | 0.0610 |
| -50 | 5.12 | 0.0970 | 85 | 2.53 | 0.0480 |
| -45 | 9.98 | 0.1900 | 90 | 1.25 | 0.0240 |
| -40 | 15.15 | 0.2920 | 95 | 0.73 | 0.0140 |
| -35 | 21.98 | 0.4350 | 100 | 0.47 | 0.0090 |
| -30 | 30.10 | 0.6250 | 105 | 0.28 | 0.0050 |
| -25 | 38.22 | 0.8490 | 110 | 0.10 | 0.0020 |
| -20 | 46.93 | 1.1530 | 115 | 0.00 | 0.0000 |

Values are average of 6-time measurements.

Table 11 Torque (N・cm)

| | z-cordinate (cm) | | | | | |
|---|---|---|---|---|---|---|
| | -100 gantry center | -90 | -80 | -70 | -60 | -50 |
| materal | | | | | | |
| Hair pin | 5.8 | 5.8 | 5.8 | 5.8 | 5.8 | 5.8 |
| Paper clip | 2.4 | 2.4 | 2.4 | 2.4 | 2.4 | 2.4 |
| SS achwire (TRU-CHROME .017x.25) 3cm | 0.1 | 0.1 | 0.1 | 0.1 | 0.1 | 0.1 |
| SS achwire (FLY .017x.025) 3cm | 0.1 | 0.1 | 0.1 | 0.1 | 0.1 | 0.1 |
| SS achwire (SHOFU) 3cm | 0.1 | 0.1 | 0.1 | 0.1 | 0.1 | 0.1 |
| SS achwire (3M) 3cm | 0.1 | 0.1 | 0.1 | 0.1 | 0.1 | 0.1 |
| SS achwire (FLY .016x.016) 3cm | 0.1 | 0.1 | 0.1 | 0.1 | 0.1 | 0.1 |
| SS achwire (Ormco) 3cm | 0.0 | 0.0 | 0.0 | 0.0 | 0.0 | 0.0 |
| SS achwire (TRU-CHROME .016x.016) 3cm | 0.0 | 0.0 | 0.0 | 0.0 | 0.0 | 0.0 |
| Ti-Nb archwire (GUMMETAL® ) 3cm | 0.0 | 0.0 | 0.0 | 0.0 | 0.0 | 0.0 |
| Co-Cr-Ni-Mo (ELGILOY® ) archwire 3cm | 0.0 | 0.0 | 0.0 | 0.0 | 0.0 | 0.0 |
| BENDALOY® Ni-Ti archwire 3 cm | 0.0 | 0.0 | 0.0 | 0.0 | 0.0 | 0.0 |
| ORTHONOL® Ni-Ti EXTENSION SPRING | 0.0 | 0.0 | 0.0 | 0.0 | 0.0 | 0.0 |
| MAXILLARY QUAD HELIX (RICKETS®) size 3 | 0.0 | 0.0 | 0.0 | 0.0 | 0.0 | 0.0 |

Values are average of 6-time measurements.